Journal of Computational Physics 350 (2017) 237–259

Contents lists available at ScienceDirect

Journal of Computational Physics

www.elsevier.com/locate/jcp

Unified gas-kinetic scheme for diatomic molecular flow with translational, rotational, and vibrational modes

Zhao Wang [a], Hong Yan [a,b,*], Qibing Li [c], Kun Xu [d]

[a] School of Power and Energy, Northwestern Polytechnical University, 127 Youyi Xilu, Xi'an, Shaanxi, 710072, China
[b] Collaborative Innovation Center for Advanced Aero-Engine, Beijing 100191, China
[c] Department of Engineering Mechanics, Tsinghua University, Beijing 100084, China
[d] Department of Mathematics, Hong Kong University of Science and Technology, Hong Kong

ARTICLE INFO

Article history:
Received 23 November 2016
Received in revised form 10 June 2017
Accepted 22 August 2017
Available online 30 August 2017

Keywords:
Unified gas-kinetic scheme
Diatomic molecules
Vibrational relaxation
Non-equilibrium hypersonic flows

ABSTRACT

The unified gas-kinetic scheme (UGKS) is a direct modeling method for both continuum and rarefied flow computations. In the previous study, the UGKS was developed for diatomic molecular simulations with translation and rotational motions. In this paper, a UGKS with non-equilibrium translational, rotational, and vibrational degrees of freedom, will be developed. The new scheme is based on the phenomenological gas dynamics model, where the translational, rotational, and vibrational modes get to the equilibrium with different time scales with the introduction of rotational and vibrational collision numbers. This new scheme is tested in a few cases, such as the homogeneous flow relaxation, shock structure, shock tube problem, and flow passing through a circular and semi-circular cylinders. The analytical and DSMC solutions are used for the validation of the UGKS, and reasonable agreements have been achieved.

1. Introduction

Hypersonic flow around a flying vehicle in near space is a typical multiple scale flow problem, where the flow physics in different regions around the vehicle can lie in different flow regimes. For example, at Mach number 4 and Reynolds number 59373, the local Knudsen number around a flying vehicle, which is defined as the ratio of local particle mean free path over the length scale of flow variable variation [1], can cover a wide range of values with five order of magnitude difference [2]. The development of multiple scale method in aerospace application seems necessary. Generally, the non-equilibrium in the hypersonic gas dynamics includes the following two aspects: (1) The translational non-equilibrium gas distribution function with highly non-equilibrium form, such as the bimodal distributions and prominent surface slip phenomena [3–5]. The translational non-equilibrium is the most difficult part to be captured. (2) The associated thermodynamic non-equilibrium related to the internal degrees of freedom, such as energy exchange among translational, rotational, and vibrational ones, and even the chemical reaction [6–8].

The study of vibrational relaxation of diatomic molecules is fundamental to the evaluation of dynamic properties of high temperature flow field [9–11]. Such studies are important not only for understanding the vibrational non-equilibrium process itself, but also for allowing to appropriately treat the strong coupling between vibrational relaxation and other non-equilibrium processes, such as dissociation, ionization, and radiation in hypersonic flight.

* Corresponding author at: School of Power and Energy, Northwestern Polytechnical University, 127 Youyi Xilu, Xi'an, Shaanxi, 710072, China.
E-mail addresses: wzhao@mail.nwpu.edu.cn (Z. Wang), yanhong@nwpu.edu.cn (H. Yan), lqb@tsinghua.edu.cn (Q. Li), makxu@ust.hk (K. Xu).

http://dx.doi.org/10.1016/j.jcp.2017.08.045
0021-9991/

Several approaches have been routinely used to solve the hypersonic rarefied flow problem. The direct simulation Monte Carlo (DSMC) method can model the non-equilibrium physics, but it becomes increasingly expensive as the Knudsen number approaches to the lower end of the transition regime. On the other hand, the traditional computational fluid dynamics (CFD) solution based on the continuity assumption starts to deteriorate as the flow goes into the transition regime [12]. The direct Boltzmann solver [13] is hampered by the difficulty of incorporating non-equilibrium flow physics, such as rotational and vibrational energy exchange, into the complete collision integral term, and is extremely expensive in terms of computational cost.

The Bhatnagar–Gross–Krook (BGK) model of the Boltzmann equation provides a viable model to solve the non-equilibrium flow problem because of its simple formulation and easy modeling for the multi-temperature non-equilibrium effect [12]. Recently, a unified gas-kinetic scheme (UGKS) has been developed for the whole Knudsen number regime based on the gas-kinetic BGK model, with discretized particle velocity space [14]. The critical step is that an integral solution of the kinetic model equation is used in the flux construction across a cell interface. The integral solution describes the scale-dependent physical process from the kinetic particle free transport to the hydrodynamic equilibrium state formation. Therefore, the integral solution gives an accurate representation for both continuum and free molecular flows. Many other conventional kinetic solvers use an operator-splitting technique. This decoupled numerical treatment, same as the DSMC method, requires a cell size and time step to resolve the solution in the particle mean free path and collision time scales, even in the continuum flow regime. Otherwise, the dissipation proportional to the particle free transport length scale, such as the cell size, will become much larger than the physical one which is on the order of particle mean free path. The UGKS is a finite volume scheme which describes a gas evolution process in a scale of the numerical time step, which can be less and much larger than the local particle time in the rarefied and continuum regimes. In the continuum flow regime at high Reynolds number, same as the macroscopic NS solver, the UGKS can use the mesh size and time step which are much larger than the particle mean free path and collision time in the capturing of the NS solutions, such as the laminar boundary layer [15].

In the previous study, the UGKS based on the BGK and Shakhov models has been developed for monatomic gas in the whole flow regimes [16–19]. For the BGK model, the Prandtl number is unit. In order to correct the heat flux with a proper Prandtl number, many generalized BGK-type kinetic models have been developed. One of the well-knowns is the Shakhov model [20]. In addition, the UGKS based on the Rykov model was developed for diatomic gas [21]. In the diatomic gas modeling, the rotational degrees of freedom were included for capturing the energy exchange between translational and rotational energy through relaxation process. More specifically, the Rykov kinetic model was used to construct the time evolution solution of a gas distribution function for the flux evaluation [22].

As described above, the study of vibrational relaxation of diatomic molecules is fundamental to the evaluation of dynamic properties of high temperature flow field. Thus, the attempt to include the vibrational mode into the UGKS has been conducted. In a recent work by Zhang [23], a model with vibrational relaxation was proposed. In this paper, we will present a UGKS for non-equilibrium flow simulation with translational, rotational, and vibrational degrees of freedom. The model used here for the construction of UGKS is a phenomenological one, which is similar to the Larsen–Borgnakke model used in DSMC [1]. The construction of vibrational degrees of freedom, and the energy exchanges between different modes, will be presented in detail. This paper is organized in the following. The UGKS is presented in Section 2. Section 3 includes five numerical test cases to validate the proposed method. The last section is the concluding remarks.

2. UGKS for diatomic molecules with vibrational relaxation

2.1. Gas-kinetic model

For diatomic gas, besides the translational degrees of freedom, the rotational and vibrational degrees of freedom are included as well in a gas distribution function, i.e., $f(t,\vec{x},\vec{u},\epsilon_r,\epsilon_v)$, where ϵ_r and ϵ_v are the rotational and vibrational energy, respectively; $\vec{x}$ and $\vec{u}$ are physical space and particle velocity space,respectively; t is time. The relations between the distribution function and macroscopic flow variables are defined as

$$\rho = \int f du dv dw d\epsilon_r d\epsilon_v,$$

$$U_i = \frac{1}{\rho}\int u_i f du dv dw d\epsilon_r d\epsilon_v,$$

$$P_{ij} = \int c_i c_j f du dv dw d\epsilon_r d\epsilon_v,$$

$$nkT_{tran} = \frac{1}{3}\int c^2 f du dv dw d\epsilon_r d\epsilon_v,$$

$$nkT_{rot} = \int \frac{\epsilon_r}{m} f du dv dw d\epsilon_r d\epsilon_v,$$

$$\frac{K_v}{2} nkT_{vib} = \int \frac{\epsilon_v}{m} f du dv dw d\epsilon_r d\epsilon_v,$$

$$q_i = \int c_i(\frac{c^2}{2} + \frac{\epsilon_r}{m} + \frac{\epsilon_v}{m}) f du dv dw d\epsilon_r d\epsilon_v \tag{1}$$

where $\vec{c} = (u - U, v - V, w - W)$ is the peculiar velocity, m is the molecular mass, n is the molecular number density, U_i is the i-direction flow velocity, P_{ij} is the stress, k is Boltzmann constant, K_v is the vibrational degree of freedom, T_{tran} is the translational temperature, T_{rot} is the rotational temperature, T_{vib} is the vibrational temperature, and q_i is the heat flux related to translational, rotational and vibrational degrees of freedom.

In order to simplify the collisional model of the full Boltzmann equation, many kinetic models were proposed and used in the study of rarefied flows [20,24–28]. For diatomic gases, the non-equilibrium vibrational, rotational, and transitional energy should be included. Attempts have been done to construct the kinetic models and develop the corresponding gas-kinetic schemes [29–32].

The model used in the construction of the UGKS with vibrational mode is a phenomenological one, which basically includes different time scales in the translational, rotational, and vibrational relaxations. A two-dimensional formulation is considered, which has the following form.

$$\frac{\partial f}{\partial t} + u\frac{\partial f}{\partial x} + v\frac{\partial f}{\partial y} = \frac{g_{tran} - f}{\tau} + \frac{g_{rot} - g_{tran}}{\tau Zr^*} + \frac{g_{vib} - g_{rot}}{\tau Zv^*}. \tag{2}$$

The collision operator on the right-hand of the equation is consisted of three terms corresponding to the translational relaxation, rotational relaxation, and vibrational relaxation,respectively. In Eq. (2), g_{tran} is the equilibrium state for the translational relaxation process with individual temperatures, g_{rot} is the equilibrium state for the translational and rotational energy exchange with two independent temperature, and g_{vib} is the final equilibrium state with a single temperature for the energy exchange among all degrees of freedom, translation, rotation, and vibration. The equilibrium states are expressed as

$$\begin{aligned}
g_{tran} &= \rho(\frac{m}{2\pi kT_{tran}})^{\frac{3}{2}} e^{-\frac{mc^2}{2kT_{tran}}} \frac{1}{kT_{rot}} e^{-\frac{\epsilon_r}{kT_{rot}}} \frac{1}{\Gamma(K_v/2)} \frac{\epsilon_v^{K_v/2-1}}{(kT_{vib})^{K_v/2}} e^{-\frac{\epsilon_v}{kT_{vib}}} \Upsilon(\lambda_{tran}),\\
g_{rot} &= \rho(\frac{m}{2\pi kT_1})^{\frac{3}{2}} e^{-\frac{mc^2}{2kT_1}} \frac{1}{kT_1} e^{-\frac{\epsilon_r}{kT_1}} \frac{1}{\Gamma(K_v/2)} \frac{\epsilon_v^{K_v/2-1}}{(kT_{vib})^{K_v/2}} e^{-\frac{\epsilon_v}{kT_{vib}}} \Upsilon(\lambda_1),\\
g_{vib} &= \rho(\frac{m}{2\pi kT})^{\frac{3}{2}} e^{-\frac{mc^2}{2kT}} \frac{1}{kT} e^{-\frac{\epsilon_r}{kT}} \frac{1}{\Gamma(K_v/2)} \frac{\epsilon_v^{K_v/2-1}}{(kT)^{K_v/2}} e^{-\frac{\epsilon_v}{kT}} \Upsilon(\lambda),
\end{aligned} \tag{3}$$

with

$$\begin{aligned}
\Upsilon &= [1 + \frac{4}{5}(1 - Pr)\lambda^2 \frac{\vec{q}\cdot\vec{c}}{\rho}(2\lambda c^2 - 5)],\\
\Gamma(j) &= \int_0^\infty x^{j-1} e^{(-x)} dx,
\end{aligned}$$

where Pr is the Prandtl number, $R = k/m$ is the gas constant, $\lambda = m/2kT$, $\tau = \mu(T_{tran})/p_{tran}$ is the relaxation time, $\mu(T_{tran})$ is the viscosity coefficient of a diatomic gas, p_{tran} is the pressure, T_1 is the equilibrium temperature for translation and rotation, and T is the equilibrium temperature for all degrees of freedom. The relaxation time τ depends on translational temperature T_{tran}, because the translational temperature characterizes the relative velocity between colliding particles. Here Zr^* is the rotational collision number, and is related to the number of collisions for the equilibrium state between the translational and rotational temperatures, and Zv^* is the corresponding vibrational collision number in the vibrational mode. The above kinetic equation follows the similar consideration of Larsen–Borgnakke model, which is used in the DSMC method [1].

2.2. Reduced gas-kinetic model

The UGKS is a scheme for capturing the time evaluation of a gas distribution function $f(t, \vec{x}, \vec{u}, \epsilon_r, \epsilon_v)$, in which the particle velocity space $\vec{u}$ is discretized, while the energy ϵ_r and ϵ_v are considered in a continuous space. In order to reduce the computational cost, reduced gas distribution functions [33] are used in the computation, and defined as,

$$\begin{aligned}
H &= \int f dw d\epsilon_r d\epsilon_v, B = \int w^2 f dw d\epsilon_r d\epsilon_v,\\
R &= \int \frac{2\epsilon_r}{m} f dw d\epsilon_r d\epsilon_v, G = \int \frac{2\epsilon_v}{m} f dw d\epsilon_r d\epsilon_v.
\end{aligned} \tag{4}$$

As a result, the relationship between the macroscopic flow variables and distribution functions can be written in terms of the moments of H, B, R and G,

$$\mathbf{W}=\begin{pmatrix}\rho\\ \rho U\\ \rho V\\ \rho E\\ \rho E_{rot}\\ \rho E_{vib}\end{pmatrix}=\int\begin{pmatrix}H\\ uH\\ vH\\ \frac{u^2+v^2}{2}H+\frac{1}{2}B+\frac{1}{2}R+\frac{1}{2}G\\ \frac{1}{2}R\\ \frac{1}{2}G\end{pmatrix}dudv. \tag{5}$$

Multiplying Eq. (2) by vector $(1, w^2, \frac{2\epsilon_r}{m}, \frac{2\epsilon_v}{m})^T$ and integrating the vector equation, the following system is obtained,

$$\frac{\partial\Phi}{\partial t}+u\frac{\partial\Phi}{\partial x}+v\frac{\partial\Phi}{\partial y}=\frac{1}{\tau}(\Phi_{eq}-\Phi), \tag{6}$$

where $\Phi=(H, B, R, G)^T$ and

$$\begin{pmatrix}H_{eq}\\ B_{eq}\\ R_{eq}\\ G_{eq}\end{pmatrix}=\nu_{tran}\begin{pmatrix}H_{tran}\\ B_{tran}\\ R_{tran}\\ G_{tran}\end{pmatrix}+\nu_{rot}\begin{pmatrix}H_{rot}\\ B_{rot}\\ R_{rot}\\ G_{rot}\end{pmatrix}+\nu_{vib}\begin{pmatrix}H_{vib}\\ B_{vib}\\ R_{vib}\\ G_{vib}\end{pmatrix}, \tag{7}$$

with $\nu_{tran}=1-1/Zr^*$, $\nu_{rot}=1/Zr^*-1/Zv^*$, $\nu_{vib}=1/Zv^*$,

$$\begin{aligned}
&H_{tran}=H_{tran,Gaussian}\cdot Y_1(\lambda_{tran}),\quad H_{rot}=H_{rot,Gaussian}\cdot Y_1(\lambda_1),\quad H_{vib}=H_{vib,Gaussian}\cdot Y_1(\lambda),\\
&B_{tran}=B_{tran,Gaussian}\cdot Y_2(\lambda_{tran}),\quad B_{rot}=B_{rot,Gaussian}\cdot Y_2(\lambda_1),\quad B_{vib}=B_{vib,Gaussian}\cdot Y_2(\lambda),\\
&R_{tran}=R_{tran,Gaussian}\cdot Y_1(\lambda_{tran}),\quad R_{rot}=R_{rot,Gaussian}\cdot Y_1(\lambda_1),\quad R_{vib}=R_{vib,Gaussian}\cdot Y_1(\lambda),\\
&G_{tran}=G_{tran,Gaussian}\cdot Y_1(\lambda_{tran}),\quad G_{rot}=G_{rot,Gaussian}\cdot Y_1(\lambda_1),\quad G_{vib}=G_{vib,Gaussian}\cdot Y_1(\lambda).
\end{aligned} \tag{8}$$

$$\begin{aligned}
&H_{tran,Gaussian}=\rho(\frac{\lambda_{tran}}{\pi})e^{-\lambda_{tran}((u-U)^2+(v-V)^2)},\\
&H_{rot,Gaussian}=\rho(\frac{\lambda_1}{\pi})e^{-\lambda_1((u-U)^2+(v-V)^2)},\\
&H_{vib,Gaussian}=\rho(\frac{\lambda}{\pi})e^{-\lambda((u-U)^2+(v-V)^2)},\\
&B_{tran,Gaussian}=\frac{K}{2\lambda_{tran}}H_{tran,Gaussian},\quad B_{rot,Gaussian}=\frac{K}{2\lambda_1}H_{rot,Gaussian},\quad B_{vib,Gaussian}=\frac{K}{2\lambda}H_{vib,Gaussian},\\
&R_{tran,Gaussian}=\frac{K_r}{2\lambda_{rot}}H_{tran,Gaussian},\quad R_{rot,Gaussian}=\frac{K_r}{2\lambda_1}H_{rot,Gaussian},\quad R_{vib,Gaussian}=\frac{K_r}{2\lambda}H_{vib,Gaussian},\\
&G_{tran,Gaussian}=\frac{K_v}{2\lambda_{vib}}H_{tran,Gaussian},\quad G_{rot,Gaussian}=\frac{K_v}{2\lambda_{vib}}H_{rot,Gaussian},\quad G_{vib,Gaussian}=\frac{K_v}{2\lambda}H_{vib,Gaussian}.
\end{aligned} \tag{9}$$

$$\begin{aligned}
&Y_1(\lambda)=1+\frac{4}{5}(1-Pr)\lambda^2\frac{[(u-U)\cdot q_x+(v-V)\cdot q_y]}{\rho}(2\lambda[(u-U)^2+(v-V)^2)]+K-5),\\
&Y_2(\lambda)=1+\frac{4}{5}(1-Pr)\lambda^2\frac{[(u-U)\cdot q_x+(v-V)\cdot q_y]}{\rho}(2\lambda[(u-U)^2+(v-V)^2)]+K-3),
\end{aligned} \tag{10}$$

where $\lambda=m/(2kT)$, K is the translational internal degree of freedom, K_r is the rotational degree of freedom. The construction of UGKS flux function for diatomic gas with vibrational relaxation is based on Eq. (6).

2.3. Unified gas-kinetic scheme

The unified gas-kinetic scheme is a finite volume method. The physical space in 2D is divided into control volumes $\Omega_{i,j}$. The temporal discretization is denoted by t_n for the n-th time step. The particle velocity space is discretized in order to capture the non-equilibrium distribution. The discrete distribution functions in physical and velocity spaces are denoted by

$$\begin{aligned}
&H^n_{i,j}=H^n_{i,j,\alpha,\beta}=H(t_n, x_i, y_j, u_\alpha, v_\beta),\\
&B^n_{i,j}=B^n_{i,j,\alpha,\beta}=B(t_n, x_i, y_j, u_\alpha, v_\beta),\\
&R^n_{i,j}=R^n_{i,j,\alpha,\beta}=R(t_n, x_i, y_j, u_\alpha, v_\beta),\\
&G^n_{i,j}=G^n_{i,j,\alpha,\beta}=G(t_n, x_i, y_j, u_\alpha, v_\beta).
\end{aligned} \tag{11}$$

With the discrete particle velocity points, the moments of the gas distribution functions can be obtained by numerical quadrature over velocity space,

$$W_{i,j}^n = \Sigma \begin{pmatrix} \kappa H_{i,j}^n \\ \kappa H_{i,j}^n u \\ \kappa H_{i,j}^n v \\ \frac{1}{2}\kappa((u^2+v^2)H_{i,j}^n + B_{i,j}^n + R_{i,j}^n + G_{i,j}^n) \\ \frac{1}{2}\kappa R_{i,j}^n \\ \frac{1}{2}\kappa G_{i,j}^n \end{pmatrix}, \tag{12}$$

where κ is the weight of numerical quadrature. The UGKS method is constructed in the following.
(a) Integrating the model Eq. (6) over the control volume $\Omega_{i,j}$ in a physical space and in a time interval (t_n, t_{n+1}).
(b) Discretizing the time integration of collision terms using a trapezoid rule.
(c) Updating the gas distribution functions $(H_{i,j}, B_{i,j}, R_{i,j}, G_{i,j})$ and macroscopic flow variables W in the control volume $\Omega_{i,j}$.

The UGKS updates the distribution functions and flow variables in the following equations.

$$\Phi_{i,j}^{n+1} = (1+\frac{\Delta t}{2\tau^{n+1}})^{-1}[\Phi_{i,j}^n + \frac{1}{\Omega_{i,j}}\int_{t^n}^{t^{n+1}}\oint_{\partial\Omega_{i,j}} \Phi_{cf}(u,v,t)\vec{u}\cdot d\vec{S}dt + \frac{\Delta t}{2}(\frac{\Phi_{eq,i,j}^{n+1}}{\tau^{n+1}} + \frac{\Phi_{eq,i,j}^n - \Phi_{i,j}^n}{\tau^n})], \tag{13}$$

$$W_{i,j}^{n+1} = W_{i,j}^n + \frac{1}{\Delta x}(\vec{F}_{i-1/2,j} - \vec{F}_{i+1/2,j}) + \frac{1}{\Delta y}(\vec{F}_{i,j-1/2} - \vec{F}_{i,j+1/2}) + S, \tag{14}$$

with

$$S = \begin{pmatrix} 0,0,0,0, \Delta t(\frac{(\rho E_{rot,eq})_{i,j}^n - (\rho E_{rot})_{i,j}^n}{2\tau^n} + \frac{(\rho E_{rot,eq})_{i,j}^{n+1} - (\rho E_{rot})_{i,j}^{n+1}}{2\tau^{n+1}}), \\ \Delta t(\frac{(\rho E_{vib,eq})_{i,j}^n - (\rho E_{vib})_{i,j}^n}{2\tau^n} + \frac{(\rho E_{vib,eq})_{i,j}^{n+1} - (\rho E_{vib})_{i,j}^{n+1}}{2\tau^{n+1}}) \end{pmatrix}^T,$$

$$\vec{F}_{i-1/2} = \int_{t^n}^{t^{n+1}}\int u(\psi_1 H_{i-1/2} + \psi_2 B_{i-1/2} + \psi_3 R_{i-1/2} + \psi_4 G_{i-1/2})dudvdt,$$

$$\vec{F}_{j-1/2} = \int_{t^n}^{t^{n+1}}\int v(\psi_1 H_{j-1/2} + \psi_2 B_{j-1/2} + \psi_3 R_{j-1/2} + \psi_4 G_{j-1/2})dudvdt,$$

$$\psi_1 = (1, u, v, \frac{1}{2}(u^2+v^2), 0, 0)^T,$$

$$\psi_2 = (0,0,0,\frac{1}{2},0,0)^T,$$

$$\psi_3 = (0,0,0,\frac{1}{2},\frac{1}{2},0)^T,$$

$$\psi_4 = (0,0,0,\frac{1}{2},0,\frac{1}{2})^T,$$

where $\vec{S}$ is the unit vector of a cell interface. $\Phi_{i,j}^{n+1}$ and $\Phi_{i,j}^n$ are the averaged reduced velocity distribution functions in the cell (i,j) at times t^{n+1} and t^n, respectively. Δt is the time step, τ^n and τ^{n+1} are relaxation times. $\Phi_{cf}(u,v,t)$ is the time-dependent reduced gas distribution function at the cell interface, which plays a central role for the capturing multiple scale flow physics in UGKS. Φ_{eq} is obtained from Eq. (9), and $\rho E_{rot,eq}$ and $\rho E_{vib,eq}$ are determined from Eqs. (5) and (9).

In the above system, in order to update the gas distribution functions in Eq. (13), Φ_{eq}^{n+1} depends on the macroscopic flow variables at $(n+1)$-th step, which can be provided through the solution of Eq. (14). Therefore, the solutions in Eqs. (13) and (14) are uniquely determined once the time dependent gas distribution functions for H, B, R, G at a cell interface are obtained. The construction of the time-dependent gas distribution function at the cell interface is the central ingredient for the development of UGKS.

In UGKS method, the time-dependent distribution function H at the cell interface is modeled by the local analytical solution of kinetic equation (Eq. (6)). A directional splitting scheme is developed in this paper. For a 2D flow, the kinetic equation, for example, in the x-direction, becomes,

$$\frac{\partial H}{\partial t}+u\frac{\partial H}{\partial x}=\frac{1}{\tau}(H_{eq}-H). \tag{15}$$

Taking the interface $x_{i+1/2}=0$ and $t_n=0$, the time evolution solution is

$$H(0,t,u_\alpha)=\frac{1}{\tau}\int_{t^n}^{t}H_{eq}(x',t',u_\alpha)e^{-(t-t')/\tau}dt'+e^{-t/\tau}H_0(-u_\alpha t,0,u_\alpha). \tag{16}$$

The initial distribution function H_0 around the interface is,

$$H_0(x,0,u_\alpha)=\begin{cases}H^L_{i+1/2,\alpha}+\sigma^H_{i,\alpha}x, & x\le 0,\\ H^R_{i+1/2,\alpha}+\sigma^H_{i+1,\alpha}x, & x>0,\end{cases} \tag{17}$$

where $H^L_{i+1/2,\alpha}$ and $H^R_{i+1/2,\alpha}$ are the reconstructed initial distribution functions on the left and right sides of the interface. Thus,

$$H^L_{i+1/2,\alpha}=H_{i,\alpha}+(x_{i+1/2}-x_i)\sigma^H_{i,\alpha},$$
$$H^R_{i+1/2,\alpha}=H_{i+1,\alpha}+(x_{i+1}-x_{i/2})\sigma^H_{i+1,\alpha},$$

where $\sigma^H_{i,\alpha}$ is the slope of H at the i-th cell and α-th particle velocity. The van Leer limiter is used for the reconstruction,

$$\sigma^H_{i,\alpha}=(\mathrm{sign}(s_1)+\mathrm{sign}(s_2))\frac{|s_1||s_2|}{|s_1|+|s_2|}, \tag{18}$$

with $s_1=(H_{i,\alpha}-H_{i-1,\alpha})/(x_i-x_{i-1})$, $s_2=(H_{i+1,\alpha}-H_{i,\alpha})/(x_{i+1}-x_i)$, and the signal function $\mathrm{sign}(s_1)$.

The Maxwellian distribution around the interface is approximated by Taylor expansion,

$$\begin{aligned}H_{eq}(x,t,u_\alpha)=&v_{tran}H_{tran}+[(1-H[x])a^L_Hx+H[x]a^R_Hx+A_Ht]H_{tran,Gaussian}\\&+v_{rot}H_{rot}+[(1-H[x])b^L_Hx+H[x]b^R_Hx+B_Ht]H_{rot,Gaussian}\\&+v_{vib}H_{vib}+[(1-H[x])c^L_Hx+H[x]c^R_Hx+C_Ht]H_{vib,Gaussian},\end{aligned} \tag{19}$$

where $H_{tran,Gaussian}$,$H_{rot,Gaussian}$, and $H_{vib,Gaussian}$ are the Maxwellian distributions at $(x=0,t=0)$, H_{tran},H_{rot}, and H_{vib} are the modified Maxwellian distributions at $(x=0,t=0)$, and $H[x]$ is the Heaviside function. Here $a^L_H, a^R_H, A_H, b^L_H, b^R_H, B_H, c^L_H, c^R_H$, and C_H are the spatial and temporal gradients for the equilibrium distribution function, and of the same form [14],

$$a=a_1+a_2u+a_3v+a_4\frac{1}{2}(u^2+v^2), \tag{20}$$

and a_1,a_2,a_3,a_4 are local constants. How to determine the above spatial and temporal gradients for the equilibrium distribution function was explained in [14].

Inserting Eq. (17) and Eq. (19) into Eq. (16), one obtains,

$$\begin{aligned}H(0,t,u_\alpha)=&v_{tran}\Big[(1-e^{-t/\tau})H_{tran}+(\tau(-1+e^{-t/\tau})+te^{-t/\tau})[a^L_HH[u_\alpha]+a^R_H(1-H[u_\alpha])\\&H_{tran,Gaussian}+\tau(t/\tau-1+e^{-t/\tau})A_HH_{tran,Gaussian}\Big]\\&+v_{rot}\Big[(1-e^{-t/\tau})H_{rot}+(\tau(-1+e^{-t/\tau})+te^{-t/\tau})[b^L_HH[u_\alpha]+b^R_H(1-H[u_\alpha])\\&H_{rot,Gaussian}+\tau(t/\tau-1+e^{-t/\tau})B_HH_{rot,Gaussian}\Big]\\&+v_{vib}\Big[(1-e^{-t/\tau})H_{vib}+(\tau(-1+e^{-t/\tau})+te^{-t/\tau})[c^L_HH[u_\alpha]+c^R_H(1-H[u_\alpha])\\&H_{vib,Gaussian}+\tau(t/\tau-1+e^{-t/\tau})C_HH_{vib,Gaussian}\Big]\\&+e^{-t/\tau}((H^L_{i+1/2,\alpha}-u_\alpha t\sigma^H_{i,\alpha})H[u_\alpha]+(H^R_{i+1/2,\alpha}-u_\alpha t\sigma^H_{i+1,\alpha})(1-H[u_\alpha])).\end{aligned} \tag{21}$$

Similar procedure is taken for the computations of B,R,G at a cell interface.

In the above cell interface distribution functions, the spatial and temporal gradients in the equilibrium states, such as for H, need to be determined

$$a^L_H=(\partial H_{tran,Gaussian}/\partial x)/H_{tran,Gaussian}=a^L_{H,1}+a^L_{H,2}u+a^L_{H,3}v+a^L_{H,4}\frac{1}{2}(u^2+v^2),$$

$$A^L_H=(\partial H_{tran,Gaussian}/\partial t)/H_{tran,Gaussian}=A^L_{H,1}+A^L_{H,2}u+A^L_{H,3}v+A^L_{H,4}\frac{1}{2}(u^2+v^2).$$

Suppose αH represents the spatial and temporal gradients of the equilibrium state H, with the coefficients $\alpha = \alpha_1 + \alpha_2 u + \alpha_3 v + \alpha_4 \frac{1}{2}(u^2 + v^2)$. These coefficients are related to the spatial and temporal derivatives of macroscopic flow variables, such as ρ', U', V', λ' for the derivatives of ρ, U, V, λ. The determination of the derivatives of the macroscopic flow variables in space and time will be shown later. The connections between the coefficients α and derivatives of ρ', U', V', λ' are the following,

$$\begin{aligned}
\alpha_1 &= \frac{2\lambda\rho' + \rho(-4\lambda^2(UU' + VV') + (2 - 2(U^2 + V^2)\lambda)\lambda')}{2\rho\lambda}, \\
\alpha_2 &= 2(\lambda U' + \lambda' U), \\
\alpha_3 &= 2(\lambda V' + \lambda' V), \\
\alpha_4 &= -2\lambda',
\end{aligned} \tag{22}$$

where $\lambda = m/(2kT_{tran})$ for a_H^L, a_H^R, and A_H; and $\lambda = m/(2kT_1)$ for b_H^L, b_H^R, and B_H; $\lambda = m/(2kT)$ for c_H^L, c_H^R, and C_H. Similarly, βB for the spatial or temporal derivative of an equilibrium state B with $\beta = \beta_1 + \beta_2 u + \beta_3 v + \beta_4 \frac{1}{2}(u^2 + v^2)$, are determined by

$$\begin{aligned}
\beta_1 &= \alpha_1 - \frac{\lambda'}{\lambda}, \\
\beta_2 &= \alpha_2, \\
\beta_3 &= \alpha_3, \\
\beta_4 &= \alpha_4,
\end{aligned} \tag{23}$$

where $\lambda = m/(2kT_{tran})$ for a_B^L, a_B^R, and A_B; $\lambda = m/(2kT_1)$ for b_B^L, b_B^R, and B_B; and $\lambda = m/(2kT)$ for c_B^L, c_B^R, and C_B. Similarly, γR for the spatial or temporal derivative of an equilibrium state R with $\gamma = \gamma_1 + \gamma_2 u + \gamma_3 v + \gamma_4 \frac{1}{2}(u^2 + v^2)$, have the solutions

$$\begin{aligned}
\gamma_1 &= \alpha_1 - \frac{\lambda'}{\lambda}, \\
\gamma_2 &= \alpha_2, \\
\gamma_3 &= \alpha_3, \\
\gamma_4 &= \alpha_4,
\end{aligned} \tag{24}$$

where in α_1, $\lambda = m/(2kT_{tran})$ for a_R^L, a_R^R, and A_R; in $\frac{\lambda'}{\lambda}$, $\lambda = m/(2kT_{rot})$ for a_R^L, a_R^R, and A_R; and $\lambda = m/(2kT_1)$ for b_R^L, b_R^R, and B_R; $\lambda = m/(2kT)$ for c_R^L, c_R^R, and C_R. Similarly, χG for the spatial or temporal derivative of an equilibrium state G with $\chi = \chi_1 + \chi_2 u + \chi_3 v + \chi_4 \frac{1}{2}(u^2 + v^2)$, have

$$\begin{aligned}
\chi_1 &= \alpha_1 - \frac{\lambda'}{\lambda}, \\
\chi_2 &= \alpha_2, \\
\chi_3 &= \alpha_3, \\
\chi_4 &= \alpha_4,
\end{aligned} \tag{25}$$

where in α_1, $\lambda = m/(2kT_{tran})$ for a_G^L, a_G^R, and A_G; in $\frac{\lambda'}{\lambda}$, $\lambda = m/(2kT_{vib})$ for a_G^L, a_G^R, and A_G; in α_1,$\lambda = m/(2kT_1)$ for b_G^L, b_G^R, and B_G; in $\frac{\lambda'}{\lambda}$, $\lambda = m/(2kT_{vib})$ for b_G^L, b_G^R, and B_G; and $\lambda = m/(2kT)$ for c_G^L, c_G^R, and C_G.

The spatial derivatives of macroscopic variables inside each cell can be obtained through the reconstruction of macroscopic flow variables with the application of nonlinear limiter. Therefore, all above spatial derivatives of ρ, U, V, λ can be subsequently derived. In order to get the time derivatives for ρ, U, V, λ, we need to do the following. Taking conservative moments on Eq. (6), due to the vanishing of conservative moments of the collision term, the moments of the temporal and spatial derivatives of a distribution function are coupled,

$$\begin{aligned}
\int \Big(& \nu_{tran}[\psi_1(\frac{dH_{tran}}{dt}) + \psi_2(\frac{dB_{tran}}{dt}) + \psi_3(\frac{dR_{tran}}{dt}) + \psi_4(\frac{dG_{tran}}{dt})] \\
& + \nu_{rot}[\psi_1(\frac{dH_{rot}}{dt}) + \psi_2(\frac{dB_{rot}}{dt}) + \psi_3(\frac{dR_{rot}}{dt}) + \psi_4(\frac{dG_{rot}}{dt})] \\
& + \nu_{vib}[\psi_1(\frac{dH_{vib}}{dt}) + \psi_2(\frac{dB_{vib}}{dt}) + \psi_3(\frac{dR_{vib}}{dt}) + \psi_4(\frac{dG_{vib}}{dt})]\Big) du dv = S,
\end{aligned}$$

where $\frac{d}{dt} = \frac{\partial}{\partial t} + u\frac{\partial}{\partial x}$, $S = (0, 0, 0, 0, \frac{\rho E_{rot,eq} - \rho E_{rot}}{\tau}, \frac{\rho E_{vib,eq} - \rho E_{vib}}{\tau})^T$.

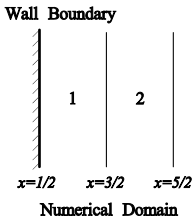

Fig. 1. Schematic of the cells adjacent to the wall.

Consequently, the temporal derivatives of macroscopic variables are obtained by

$$\partial W/\partial t = -\int \begin{pmatrix} \nu_{tran}[\psi_1 u\frac{\partial H_{tran}}{\partial x} + \psi_2 u\frac{\partial B_{tran}}{\partial x} + \psi_3 u\frac{\partial R_{tran}}{\partial x} + \psi_4 u\frac{\partial G_{tran}}{\partial x}] \\ + \nu_{rot}[\psi_1 u\frac{\partial H_{rot}}{\partial x} + \psi_2 u\frac{\partial B_{rot}}{\partial x} + \psi_3 u\frac{\partial R_{rot}}{\partial x} + \psi_4 u\frac{\partial G_{rot}}{\partial x}] \\ + \nu_{vib}[\psi_1 u\frac{\partial H_{vib}}{\partial x} + \psi_2 u\frac{\partial B_{vib}}{\partial x} + \psi_3 u\frac{\partial R_{vib}}{\partial x} + \psi_4 u\frac{\partial G_{vib}}{\partial x}] \end{pmatrix} dudv + S. \tag{26}$$

Then, along with Eq. (26), the temporal derivatives of distribution functions are fully determined using Eqs. (22)–(25).

2.4. Update of vibrational degrees of freedom

Different from the translational and rotational degrees of freedom, the vibrational degree of freedom K_v is a temperature dependent variable. So a proper determination of K_v in terms of temperature is very important. According to harmonic oscillator model, the specific vibrational energy associated with a characteristic vibrational mode temperature Θ_v is the following [1]

$$e_v = \frac{R\Theta_v}{e^{(\Theta_v/T_{vib})} - 1}. \tag{27}$$

The vibrational temperature T_{vib} can be obtained from the vibrational energy. Then, according to equal partition to each degree of freedom, the vibrational degree of freedom K_v at temperature T_{vib} can be determined by the following formula

$$K_v = \frac{2\Theta_v/T_{vib}}{e^{(\Theta_v/T_{vib})} - 1}. \tag{28}$$

2.5. Discussion on the wall boundary condition

The non-equilibrium effect is more profound near the wall, so it is necessary to discuss on the wall boundary condition. The diffusive reflection gas-surface wall condition is used. Only isothermal wall boundary condition in one dimensional case is discussed. As shown in Fig. 1, the wall ($x = 1/2$) is assumed to be on the left side. The incoming distribution function on the wall can be obtained by interpolation. For example, H_α^{in}, B_α^{in}, R_α^{in}, and G_α^{in} can be interpolated similarly from the data in the interior region,

$$H_\alpha^{in} = \frac{18H_{1,a} - 2H_{2,a} - 9\sigma_{1,a}^H\Delta x + 3\sigma_{2,\alpha}^H\Delta x}{16}, \tag{29}$$

where H_α^{in} is the reduced gas distribution function of inflow at α-th discrete particle velocity u_α. $H_{1,\alpha}$ and $H_{2,\alpha}$ are the reduced gas distribution function in cell 1 and 2 at α-th discrete particle velocity u_α respectively. $\sigma_{1,\alpha}^H$ and $\sigma_{1,\alpha}^H$ are the slope of the reduced gas distribution function H in cell 1 and 2 at α-th discrete particle velocity u_α. Δx is the cell size. Then, we can calculate the density on the wall under the condition of no particle penetrating at the wall,

$$\int_{u>0} ug_w d\Xi + \int_{u<0} uf^{in} d\Xi = 0, \tag{30}$$

where $d\Xi = dudvdwd\epsilon_r d\epsilon_v$, which gives

$$\rho_w = \frac{\Sigma_{u<0}\kappa_\alpha u_\alpha H_\alpha^{in}}{(\frac{\lambda_w}{\pi})^{1/2}\Sigma_{u>0}\kappa_\alpha u_\alpha e^{-\lambda_w(u_\alpha - U_w)^2}}, \tag{31}$$

and U_w, λ_w take the values of the wall. It is essential to emphasize that the equilibrium distribution function on the wall is as follows

$$g_w = \rho_w \left(\frac{\lambda_w}{\pi}\right)^{\frac{3}{2}} e^{-\lambda_w[(u-U_w)^2+v^2+w^2]} \frac{1}{kT_{rot,in}} e^{-\frac{\epsilon_r}{kT_{rot,in}}} \frac{1}{\Gamma(K_v/2)} \frac{\epsilon_v^{K_v/2-1}}{(kT_{vib,in})^{K_v/2}} e^{-\frac{\epsilon_v}{kT_{vib,in}}}, \tag{32}$$

where $T_{rot,in}$ and $T_{vib,in}$ are rotational and vibrational temperatures of the inflow. Due to the short collision time between the particles and the wall, the translational, rotational, and vibrational temperatures keep different values at the wall. Based on Eq. (9), the corresponding reduced Maxwellian distributions $H_\alpha^w, B_\alpha^w, R_\alpha^w$, and G_α^w on the wall are obtained. So the distribution function at the boundary interface is expressed as (same for $B_\alpha, R_\alpha, G_\alpha$)

$$H_\alpha = H_\alpha^w H[u_\alpha] + H_\alpha^{in}(1 - H[u_\alpha]). \tag{33}$$

Therefore, the fluxes of macroscopic flow variables and microscopic distribution functions on the wall can be determined by the numerical quadrature.

At end, we summarize the unified gas-kinetic scheme for diatomic gases with vibrational relaxation as follows:

1. The original kinetic model equation is split into four equations for the reduced distribution functions.
2. The time evolution of distribution functions at a cell interface is modeled by the integral solution of the kinetic model Eq. (6).
3. The initial condition and the integration of equilibrium states are determined explicitly in Eq. (16) for the flux evaluation. The macroscopic conservative flow variables inside the each cell are updated using Eq. (14).
4. A finite volume scheme is developed for the update of gas distribution functions with fluxes from Eq. (13), and with the source terms treatment inside the each cell.

2.6. Limiting solutions of UGKS in the continuum regime

In this section, we are going to analyze the UGKS with vibrational relaxation in the continuum limit at small τ, under the condition $\Delta t \gg \tau$. For the sake of simple presentation, the discussion is for the case in the one dimensional physical space. Following the Chapman–Enskog theory, at $\tau \ll 1$ the cell reduced average solutions $\Phi_i(u)$ can be formally expressed as an asymptotic expansion of small parameter,

$$\Phi_i = \Phi_i^0 + \tau \Phi_i^1 + O\left(\tau^2\right). \tag{34}$$

The modified reduced equilibrium function $\left(\Phi_{eq}\right)_i$can be expanded as

$$\left(\Phi_{eq}\right)_i = (\Phi_{Gaussian})_i + \left(\Phi^{fix}\right)_i, \tag{35}$$

where Φ^{fix} is of order τ. According to reference [15], we have

$$\begin{aligned}\Phi_{i+1/2}(t,u_\alpha) &= \Phi_{Gaussian,i+1/2,\alpha}(t) + \Phi_{i+1/2,\alpha}^{fix}(t) \\ &- \tau\left(\partial_t \Phi_{Gaussian,i+1/2,\alpha}(t) + u_\alpha \partial_x \Phi_{Gaussian,i+1/2,\alpha}(t)\right) + O\left(\tau\Delta t, \Delta t^2, \Delta x^2\right).\end{aligned} \tag{36}$$

As an example, we will analyze the reduced distribution function H first,

$$\begin{aligned}H_{i+1/2}(t,u_\alpha) &= H_{Gaussian,i+1/2,\alpha}(t) + H_{i+1/2,\alpha}^{fix}(t) \\ &- \tau\left(\partial_t H_{Gaussian,i+1/2,\alpha}(t) + u_\alpha \partial_x H_{Gaussian,i+1/2,\alpha}(t)\right) + O\left(\tau\Delta t, \Delta t^2, \Delta x^2\right).\end{aligned} \tag{37}$$

The non-equilibrium part in Eq. (37) is

$$\begin{aligned}H_{i+1/2,\alpha}^{neq} &= H_{i+1/2,\alpha}^{fix}(t) - \tau\left(\partial_t H_{Gaussian,i+1/2,\alpha}(t) + u_\alpha \partial_x H_{Gaussian,i+1/2,\alpha}(t)\right) \\ &= \nu_{tran}\left[H_{tran,i+1/2,\alpha}^{fix}(t) - \tau\left(\partial_t H_{tran,Gaussian,i+1/2,\alpha}(t) + u_\alpha \partial_x H_{tran,Gaussian,i+1/2,\alpha}(t)\right)\right] \\ &+ \nu_{rot}\left[H_{rot,i+1/2,\alpha}^{fix}(t) - \tau\left(\partial_t H_{rot,Gaussian,i+1/2,\alpha}(t) + u_\alpha \partial_x H_{rot,Gaussian,i+1/2,\alpha}(t)\right)\right] \\ &+ \nu_{vib}\left[H_{vib,i+1/2,\alpha}^{fix}(t) - \tau\left(\partial_t H_{vib,Gaussian,i+1/2,\alpha}(t) + u_\alpha \partial_x H_{vib,Gaussian,i+1/2,\alpha}(t)\right)\right] \\ &= \nu_{tran} H_{tran,i+1/2,\alpha}^{neq} + \nu_{rot} H_{rot,i+1/2,\alpha}^{neq} + \nu_{vib} H_{vib,i+1/2,\alpha}^{neq},\end{aligned} \tag{38}$$

where

$$H^{neq}_{tran,i+1/2,\alpha} = H_{tran,Gaussian,i+1/2,\alpha}(t)\frac{4(1-\Pr)\lambda^2_{tran}}{5\rho}c_\alpha\cdot q_{tran,x}\left(2\lambda_{tran}c^2_\alpha-3\right)$$
$$-H_{tran,Gaussian,i+1/2,\alpha}(t)\tau\left[\left(\lambda_{tran}c^2_\alpha-\frac{3}{2}\right)c_\alpha\cdot\frac{\partial\ln T_{tran}}{\partial x}+c_\alpha\cdot\frac{1}{p_{tran}}\frac{\partial\left(p_{tran}-\tilde{p}\right)}{\partial x}\right.$$
$$\left.+\left(\frac{mc_\alpha{}^2-kT_{tran}}{2kT^2_{tran}}\left(\varpi_1-\frac{2}{3}T_{tran}\right)+2\lambda_{tran}c^2_\alpha-1\right)\frac{\partial U}{\partial x}\right]. \tag{39}$$

Here c_α denotes the peculiar velocity, and $\tilde{p}=\nu_{tran}\left(\frac{\rho}{2\lambda_{tran}}\right)+\nu_{rot}\left(\frac{\rho}{2\lambda_1}\right)+\nu_{vib}\left(\frac{\rho}{2\lambda}\right)$. ϖ_1 is determined by the following equation,

$$\frac{2\nu_{tran}(T_{rot}-T_{tran})-2T_{rot}-K_v\nu_{vib}(T_{vib}-T)}{3}=-\frac{2T_{tran}}{3}+\varpi_1. \tag{40}$$

Subsequently, other non-equilibrium parts $H^{neq}_{rot,i+1/2,\alpha}$, $H^{neq}_{vib,i+1/2,\alpha}$ in Eq. (38) and obtained similarly.

Then the cell interface flux for the conservative variables up to $O(\tau)$ can be determined by

$$\vec{F}=\int u\left(\psi_1 H_{i+1/2}(t,u)+\psi_2 B_{i+1/2}(t,u)+\psi_3 R_{i+1/2}(t,u)+\psi_4 G_{i+1/2}(t,u)\right)du$$
$$=\begin{pmatrix}\rho U\\ \rho U^2+\tilde{p}-\frac{4}{3}\tilde{\mu}U_x-\Omega_{\rho U}\\ \left(\rho E+\tilde{p}\right)U-\frac{4}{3}\tilde{\mu}UU_x-k_hT_x(1-\Pr)-C_p\tilde{\mu}T_x-\Omega_{\rho E}\end{pmatrix}+O\left(\tau\Delta t,\Delta t^2,\Delta x^2\right). \tag{41}$$

In above equation, Prandtl number is defined as

$$Pr=C_p\tilde{\mu}/k_h, \tag{42}$$

where $C_p=\frac{7+K_v}{2}R$, k_h is heat conduction coefficient. Then, Eq. (41) becomes

$$\vec{F}=\begin{pmatrix}\rho U\\ \rho U^2+\tilde{p}-\frac{4}{3}\tilde{\mu}U_x-\Omega_{\rho U}\\ \left(\rho E+\tilde{p}\right)U-\frac{4}{3}\tilde{\mu}UU_x-k_hT_x-\Omega_{\rho E}\end{pmatrix}+O\left(\tau\Delta t,\Delta t^2,\Delta x^2\right),$$

with the viscosity coefficient $\tilde{\mu}=\tau\tilde{p}$ and heat conduction coefficient $k_h=C_p\tilde{\mu}/Pr$. In addition,

$$\Omega_{\rho U}=\frac{\tilde{\mu}U_x}{\tilde{T}}\left(\nu_{tran}\varpi_1+\nu_{rot}\varpi_2+\nu_{vib}\varpi_3\right) \tag{43}$$

and

$$\Omega_{\rho E}=R\tau\left(\nu_{tran}p_{tran}\left(T_{tran,x}-T_x\right)+\nu_{rot}p_1\left(T_{1,x}-T_x\right)\right)+\rho R\tau UU_x\left(\nu_{tran}\varpi_1+\nu_{rot}\varpi_2+\nu_{vib}\varpi_3\right)$$
$$+\tau\left[\nu_{tran}\left(\frac{\left(1+3U^2\lambda^2_{tran}\right)\left(p_{tran,x}-\tilde{p}_x\right)}{2\lambda_{tran}}\right)+\nu_{rot}\left(\frac{\left(1+3U^2\lambda^2_1\right)\left(p_{1,x}-\tilde{p}_x\right)}{4\lambda_1}\right)\right.$$
$$\left.+\nu_{vib}\left(\frac{\left(1+3U^2\lambda^2\right)\left(p_x-\tilde{p}_x\right)}{4\lambda}\right)\right], \tag{44}$$

where ϖ_2 and ϖ_3 are determined by the following two equations,

$$-\frac{2\tilde{T}+K_v\nu_{vib}(T_{vib}-T)}{5}=-\frac{2T_1}{3}+\varpi_2, \tag{45}$$

$$-\frac{2\tilde{T}}{5+K_v}=-\frac{2T}{3}+\varpi_3, \tag{46}$$

with $\tilde{T}=\tilde{p}/(\rho R)$.

Based on the above analysis, we can observe that in the continuum regime the UGKS with vibrational relaxation solves the following equations,

$$\frac{\partial\rho}{\partial t}+\frac{\partial(\rho U)}{\partial x}=O\left(\Delta t^2,\Delta x^2\right),$$
$$\frac{\partial(\rho U)}{\partial t}+\frac{\partial\left(\rho U^2+\tilde{p}-\frac{4}{3}\tilde{\mu}U_x-\Omega_{\rho U}\right)}{\partial x}=O\left(\Delta t^2,\Delta x^2\right),$$

$$\frac{\partial(\rho E)}{\partial t}+\frac{\partial\left(\left(\rho E+\tilde{p}\right)U-\frac{4}{3}\tilde{\mu}UU_x-k_hT_x-\Omega_{\rho E}\right)}{\partial x}=O\left(\Delta t^2,\Delta x^2\right), \tag{47}$$

and the above equations have the following properties:

(a). In the limit without rotational and vibrational degrees of freedom, Eq. (47) can reduce to the UGKS for monatomic gas in the NS regime. It is demonstrated as follows. When the values of Zr^* of and Zv^* are infinity,

$$\Omega_{\rho U}=\tau p_{tran}U_x\frac{\varpi_1}{T_{tran}}=0, \tag{48}$$

$$\Omega_{\rho E}=R\tau p_{tran}\left(T_{tran,x}-T_{tran,x}\right)+\rho R\tau UU_x\varpi_1+\tau\left(\frac{\left(1+3U^2\lambda_{tran}^2\right)\left(p_{tran,x}-p_{tran,x}\right)}{2\lambda_{tran}}\right)=0. \tag{49}$$

Substituting Eqs. (48) and (49) into equation (47), it becomes

$$\begin{aligned}
&\frac{\partial\rho}{\partial t}+\frac{\partial(\rho U)}{\partial x}=O\left(\Delta t^2,\Delta x^2\right),\\
&\frac{\partial(\rho U)}{\partial t}+\frac{\partial\left(\rho U^2+p-\frac{4}{3}\mu U_x\right)}{\partial x}=O\left(\Delta t^2,\Delta x^2\right),\\
&\frac{\partial(\rho E)}{\partial t}+\frac{\partial\left((\rho E+p)U-\frac{4}{3}\mu UU_x-k_hT_x\right)}{\partial x}=O\left(\Delta t^2,\Delta x^2\right),
\end{aligned} \tag{50}$$

which is the Navier–Stokes equations in 1D case [15].

(b). In the limit of total equilibrium state, and with the assumption of equal relaxation rate $Zr^*=Zv^*=1$, Eq. (47) can recover the NS equations with bulk viscosity for the rotational and vibrational degrees of freedom [34]. Eq. (47) becomes

$$\begin{aligned}
&\frac{\partial\rho}{\partial t}+\frac{\partial(\rho U)}{\partial x}=0,\\
&\frac{\partial(\rho U)}{\partial t}+\frac{\partial\left(\rho U^2+p-\frac{4}{3}\mu U_x-\Omega_{\rho U}\right)}{\partial x}=0,\\
&\frac{\partial(\rho E)}{\partial t}+\frac{\partial\left((\rho E+p)U-\frac{4}{3}\mu UU_x-k_hT_x-\Omega_{\rho E}\right)}{\partial x}=0,
\end{aligned} \tag{51}$$

where

$$\Omega_{\rho U}=\mu U_x\frac{\varpi_3}{T}=\mu U_x\left(-\frac{2}{5+K_v}+\frac{2}{3}\right), \tag{52}$$

$$\Omega_{\rho E}=\rho R\tau UU_x\varpi_3=\mu UU_x\left(-\frac{2}{5+K_v}+\frac{2}{3}\right). \tag{53}$$

Substituting Eqs. (52) and (53) into Eq. (51), the NS equations are

$$\begin{pmatrix}\rho\\ \rho U\\ \rho E\end{pmatrix}_t+\begin{pmatrix}\rho U\\ \rho U^2+p\\ (\rho E+p)U\end{pmatrix}_x=\begin{pmatrix}0\\ \frac{2K_{t,i}}{K_{t,i}+1}\tau pU_x\\ k_hT_x+\frac{2K_{t,i}}{K_{t,i}+1}\tau pUU_x\end{pmatrix}, \tag{54}$$

where $K_{t,i}$ is the total internal degrees of freedom. Obviously, Eq. (54) is the same as that in reference [34].

(c). When $1<Zr^*<\infty$, $1<Zv^*<\infty$ and different translational, rotational, and vibrational temperatures, Eq. (47) includes non-equilibrium effect beyond the NS modeling, which is an extension of the non-equilibrium modeling equations with translational and rotational degrees of freedom only [32,35]. With the temperature non-equilibrium, even in the continuum regime, the NS constitutive relationship between stress and strain is replaced by the temperature differences [30,32]. In other words, the kinetic formulation definitely provides a more general description for the gas dynamics than the NS solutions. The target of UGKS is to provide such a multiple scale non-equilibrium modeling in the continuum and rarefied regimes with a smooth transition.

3. Numerical teat cases

3.1. Rotational and vibrational relaxation in a homogeneous gas

For a diatomic homogeneous gas with different initial translational temperature T_{tran}, rotational temperature T_{rot}, vibrational temperature T_{vib}, the system can evolve into an equilibrium one with the average temperature T, which is a constant. Due to the homogeneous space distributions, the governing equation can be simplified as

$$\frac{\partial f}{\partial t} = \frac{g_{tran} - f}{\tau} + \frac{g_{rot} - g_{tran}}{\tau Zr^*} + \frac{g_{vib} - g_{rot}}{\tau Zv^*}. \tag{55}$$

Multiplying Eq. (55) with ϵ_r and ϵ_v, respectively, and integrating it over the whole velocity, rotational energy, and vibrational energy space, the time evolution of rotational energy can be obtained,

$$\frac{\partial T_{rot}}{\partial t} = \frac{T_{tr,r} - T_{rot}}{Zr^*} + \frac{T - T_{tr,r}}{\tau Zv^*}, \tag{56}$$

where $T_{tr,r}$ is the average temperature of translational and rotational temperature. The vibrational energy evolves as

$$\frac{\partial [K_v(T_{vib})T_{vib}]}{\partial t} = \frac{K_v(T)T - K_v(T_{vib})T_{vib}}{\tau Zv^*}. \tag{57}$$

If the vibrational degree of freedom is fixed, Eq. (57) can be simplified as

$$\frac{\partial T_{vib}}{\partial t} = \frac{T - T_{vib}}{\tau Zv^*}. \tag{58}$$

In the case with the constant rotational and vibrational collision numbers Zr^* and Zv^*, as well as relaxation time (r.t) τ, an analytical solution of Eqs. (56) and (58) can be obtained

$$T_{rot} = T^* - (T^* - T_{rot}(0))e^{(-t/\tau Zr^*)}, \tag{59}$$

$$T_{vib} = T - (T - T_{vib}(0))e^{(-t/\tau Zv^*)}, \tag{60}$$

where $T^* = (Zr^*/Zv^*(T - T_{tr,r}) + T_{tr,r})$. Thus, according to energy conservation, we get

$$T_{tran} = \frac{(5 + K_v)T - K_v T_{vib} - 2T_{rot}}{3}. \tag{61}$$

The critical point is to determine T and $T_{tr,r}$.

For the fixed K_v case,

$$T = \frac{Kv T_{vib}(0) + 2T_{rot}(0) + 3T_{tran}(0)}{5 + Kv}, \tag{62}$$

and

$$T_{tr,r} = \frac{2T_{rot}(0) + 3T_{tran}(0)}{5}. \tag{63}$$

For the varied K_v case,

$$T = \frac{K_v(0)T_{vib}(0) + 2T_{rot}(0) + 3T_{tran}(0)}{5 + \frac{2\Theta_v/T}{e^{(\Theta_v/T)}-1}}. \tag{64}$$

For real diatomic gas, the relaxation time depends on the translational temperature even in the homogeneous case. Using variable hard sphere (VHS) model, the relaxation time is approximated as $\tau = \mu/p_{tran} \sim T_{tran}^{\omega}/\rho R T_{tran}$, which is a constant only for the Maxwell molecule with $\omega = 1$. For nitrogen molecular ($\omega = 0.72$), depending on the temperature there is no exact analytical solution. In this test, only one cell in physical space is used. The initial rotational and vibrational temperatures are set to zero and the initial translational temperature is set to 5000 K. Fig. 2(a) shows the rotational and vibrational relaxation at $Zr^* = 5$, $Zv^* = 5$, and $K_v = 1.1$ for the Maxwell and nitrogen molecules, along with the analytical solution (Maxwell gas only). The relaxation time is calculated using the average temperature T, and used to normalize the time. The UGKS solutions for the Maxwell molecule agree well with the analytical prediction for the fixed K_v. The collision frequency for the nitrogen molecule is higher than the Maxwell one, thus presents faster relaxation to the equilibrium state. Fig. 2(b) shows rotational and vibrational relaxation for $Zr^* = 5$ and $Zv^* = 5$ with the varied K_v, in which $T = 2520$ K.

Considering the degree of freedom of the vibration is not constant, for convenience,the initial vibrational degree of freedom is given by the final equilibrium temperature,

$$K_v(0) = \frac{2\Theta_v/T}{e^{(\Theta_v/T)} - 1}. \tag{65}$$

Thus, it will tend to zero once the iteration begins because the initial vibrational temperature is zero. According to the relationship between the vibrational energy and temperature,

$$T_{vib} = \frac{e_{vib}}{\frac{1}{2}K_v R}. \tag{66}$$

The vibrational temperature T_{vib} can suddenly jump to 700 K under a certain vibrational energy. Similar phenomenon occurs in reference [1].

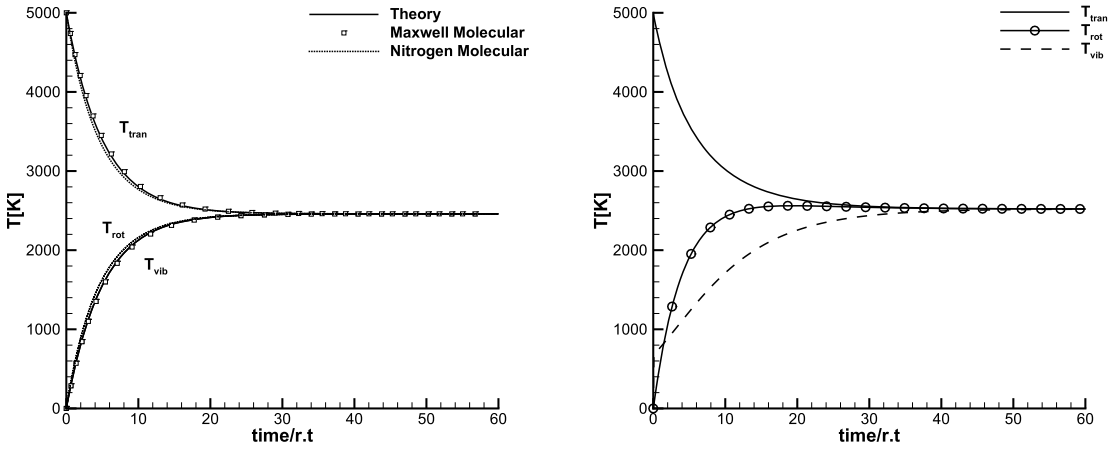

(a) case with fix K_v $(Zr^* = 5, Zv^* = 5)$ (b) case with variable K_v $(Zr^* = 5, Zv^* = 5)$

Fig. 2. Rotational and vibrational relaxation in a homogeneous gas.

3.2. 1D shock tube problem

In order to validate the model with vibrational relaxation, the solution for $Zr^* \to \infty$ and $Zv^* \to \infty$ can be obtained as a limiting solution for the monatomic gas. In the computational domain $x \in [0, L = 1800 l_{mfp}]$, 180 cells with uniform mesh in space are used, where l_{mfp} is the mean free path for the state on the left side initially. In the particle velocity space, 200 points with uniform distribution are used. The reference temperature is 1000 K. The initial conditions for the mass density, velocity, and temperature are

$$\rho_L = 1, U_L = 0, T_{tran,L} = T_{rot,L} = T_{vib,L} = 2, \quad x \le 0.5L.$$

$$\rho_R = 0.125, U_R = 0, T_{tran,R} = T_{rot,R} = T_{vib,R} = 1.6, \quad x > 0.5L.$$

For convenience, the UGKS with vibrational relaxation is denoted by UGKS-Vib in the following. As shown in Fig. 3, the solutions from the Shakhov model and UGKS-Vib model agree well when $Zr^* \to \infty$ and $Zv^* \to \infty$. The reason for the smooth connection for the rotational and vibrational temperature between two sides is that at $Zr^* = Zv^* = \infty$ the rotational and vibrational temperatures are frozen due to the absence of energy exchange between them and the translational one. Basically, both UGKS-Vib model and Shakhov model simulate monatomic gas flow as $Zr^* \to \infty$ and $Zv^* \to \infty$. Fig. 4 shows the solution of UGKS-Vib when $Zr^* = 3$ and $Zv^* = 30$. The output time for all simulations is $t = 360$.

3.3. Shock structure

To test the UGKS-Vib scheme for planar shock structures, one natural requirement is to specify the post-shock equilibrium state as the proper initial and downstream boundary condition. For diatomic molecules, because the vibrational degrees of freedom are activated under high temperature, the specific heat ratio γ is a variable across the shock wave. For this reason, we first proceed to obtain general formulations to compute the post-shock equilibrium state for diatomic or polyatomic molecules. At this post-shock equilibrium state, we assume that all temperature relaxation processes are completed.

Denoting the pre-shock as state 1 and the post-shock as state 2. The relations between these two states are as follows:

$$\frac{T_2}{T_1} = \frac{(\frac{\gamma_2}{\gamma_2 - 1} + \frac{\gamma_2}{2} M_2^2)}{(\frac{\gamma_1}{\gamma_1 - 1} + \frac{\gamma_1}{2} M_1^2)}, \tag{67}$$

$$\frac{U_2}{U_1} = \frac{M_2 \sqrt{\gamma_2 T_2}}{M_1 \sqrt{\gamma_1 T_1}}, \tag{68}$$

$$\frac{\rho_1}{\rho_2} = \frac{U_2}{U_1}. \tag{69}$$

In addition, the relation between pre-shock and post-shock Mach number is as follows

$$M_2^2 = \frac{\frac{\gamma_2^2}{\gamma_2 - 1} - 2\alpha^2 \gamma_2 - \sqrt{(\frac{\gamma_2^2}{\gamma_2 - 1})^2 - 4\alpha^2 \frac{\gamma_2^3}{\gamma_2 - 1} + 2\alpha^2 \gamma_2^2}}{2\alpha^2 \gamma_2^2 - \gamma_2^2}, \tag{70}$$

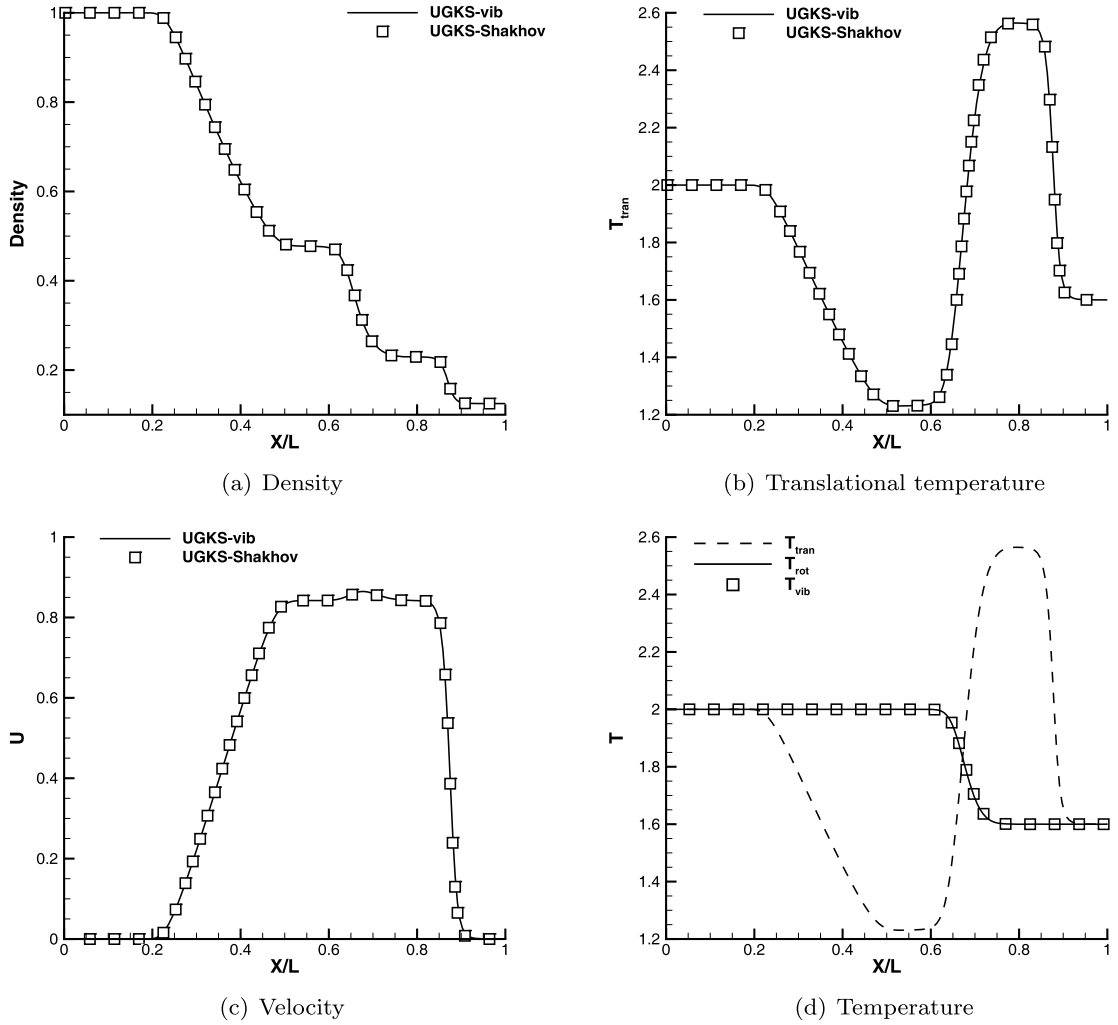

Fig. 3. UGKS-Vib solutions for shock tube ($Zr^* \to \infty$, $Zv^* \to \infty$), all x-coordinates and physical quantities are dimensionless.

where

$$\alpha = \frac{M_1(\frac{\gamma_1^2}{\gamma_1 - 1} + \frac{\gamma_1^2}{2}M_1^2)}{1 + \gamma_1 M_1^2}.$$

Although the preceding equations explicitly link the post-shock Mach number and the specific heat ratio γ_2, to solve the preceding equations, the expression for the specific heat ratio γ_2 is needed to obtain the post-shock state Mach number. So the iteration process is used to obtain the post-shock equilibrium state. The effective vibrational degree of freedom at temperature T_v can be obtained according to Eq. (28). In addition, the specific heat ratio is determined as follows,

$$\gamma = \frac{3 + K_r + K_v + 2}{3 + K_r + K_v}. \tag{71}$$

The following iteration process is used for its solution. Firstly, with a specified γ_2, use M_1 and γ_1 to compute an intermediate post-shock Mach number M_2. Secondly, use this Mach number M_2 and the specific heat ratio γ_2 to determine a post-shock temperature T_2. Thirdly, use Eqs. (28) and (71) to determine a new specific heat ratio γ_2. The above steps proceed until a converged solution is obtained.

For the nitrogen gas, the viscosity in DSMC simulation is calculated with VHS model ($\omega = 0.74$). We performed two numerical simulations of strong planar shock waves with the same free stream temperature and density, $T_\infty = 226.149$ K, $\rho_\infty = 1.7413 \times 10^{-2}$ kg/m^3, but different free stream Mach numbers: $M_\infty = 10.0, 15.0$. The thermal non-equilibrium effects are significant, and the equilibrium specific heat ratio values are $\gamma_1 = 1.399$ and $\gamma_2 = 1.3193$, and 1.3021, correspondingly. In these UGKS-Vib simulations, the specific relaxation numbers are ($Zr^* = 3$, $Zv^* = 40$) for $M_\infty = 10.0$, and ($Zr^* = 5$, $Zv^* =$

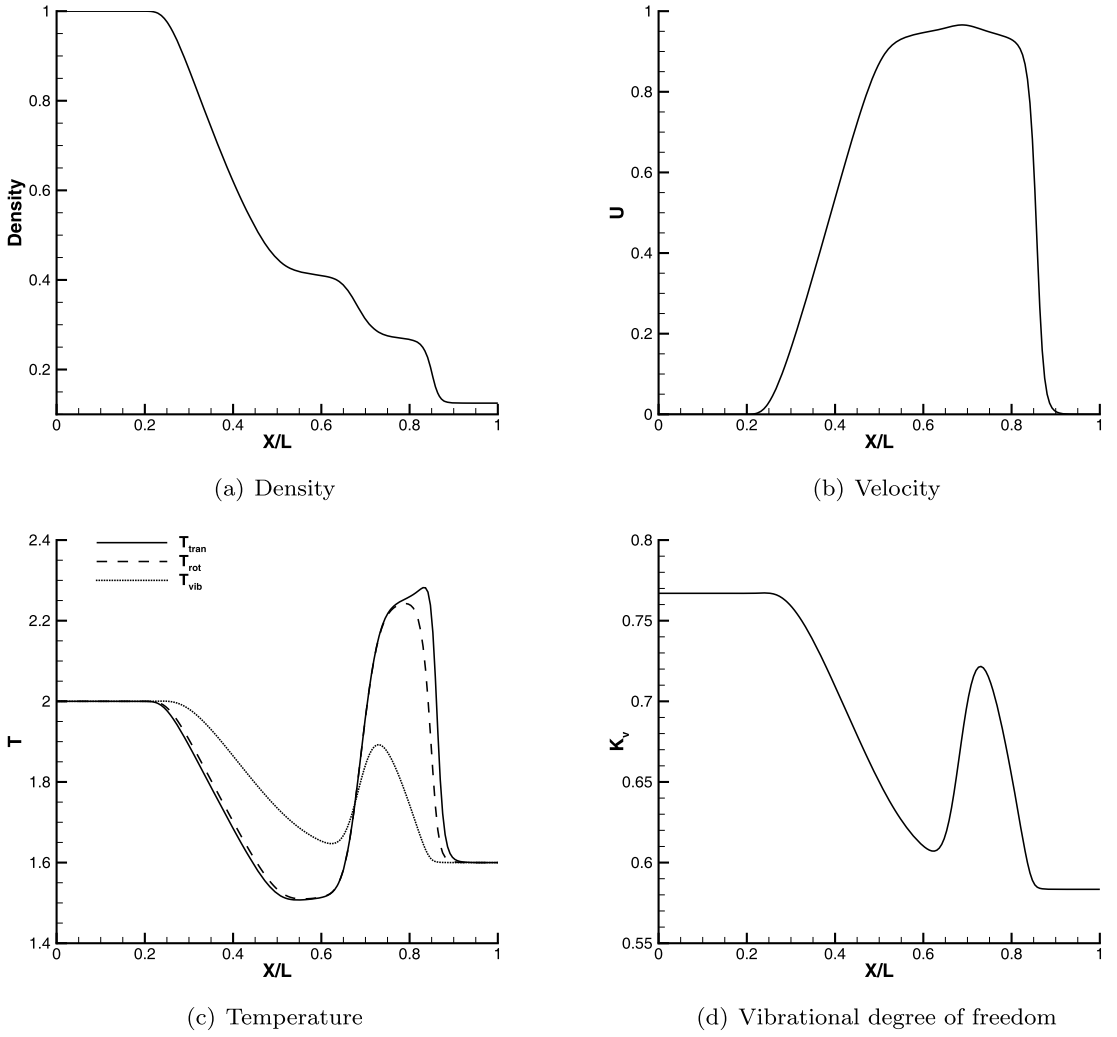

(a) Density (b) Velocity

(c) Temperature (d) Vibrational degree of freedom

Fig. 4. UGKS-Vib solutions for shock tube ($Zr^* = 3$, $Zv^* = 30$), all x-coordinates and physical quantities are dimensionless.

20) for $M_\infty = 15.0$. In the following results, density and temperature profiles are normalized by the values at the two ends of the shocks: for example, $T' = (T - T_1)/(T_2 - T_1)$. The reference mean free path and viscosity are calculated through the hard sphere model. Figs. 5–6 show the simulations results for $M_\infty = 10$ and 15 from both DSMC [12] and UGKS-Vib. It can be found that the solutions of UGKS agree well with the DSMC data.

3.4. Flow around a circular cylinder

We consider a hypersonic flow passing through a circular cylinder at $Ma = 15.0$ and $Kn = 0.01$. As shown in Fig. 7, the cylinder radius has a value of 0.04 m, and the computational domain is meshed with 40×55 quadrilateral cells for UGKS-Vib.

The inflow nitrogen gas has a velocity $U_\infty = 4511$ m/s with temperature $T_\infty = 217.5$ K, and molecule mass density $\rho_\infty = 7.48 \times 10^{-5}$ kg/m^3. The cylinder has a cold surface with a constant temperature $T_w = 1000$ K. For UGKS-Vib, the domain $(u, v) \in [-30 \times \sqrt{RT_\infty}, 30 \times \sqrt{RT_\infty}] \times [-30 \times \sqrt{RT_\infty}, 30 \times \sqrt{RT_\infty}]$ in the velocity space is discretized with 89×89 mesh points based on Newton–Cotes rule. The relaxation time is calculated with $\tau = \mu_\infty (T/T_\infty)^\omega / p_{tran}$, and the temperature exponent of the viscosity coefficient is $\omega = 0.74$. According to reference [36], the rotational and vibrational collision number are obtained as follows.

$$Zr^* = \frac{K_t}{K_t + K_r} \frac{Zr^\infty}{1 + (\pi^{1/2}/2)(T^*/T_{tran})^{1/2} + (\pi + \pi^2/4)(T^*/T_{tran})}, \tag{72}$$

$$Zv^* = \frac{K_t + K_r}{K_t + K_r + K_v} \cdot C_1 / T_{tran}^\omega \exp(C_2 T_{tran}^{-1/3}), \tag{73}$$

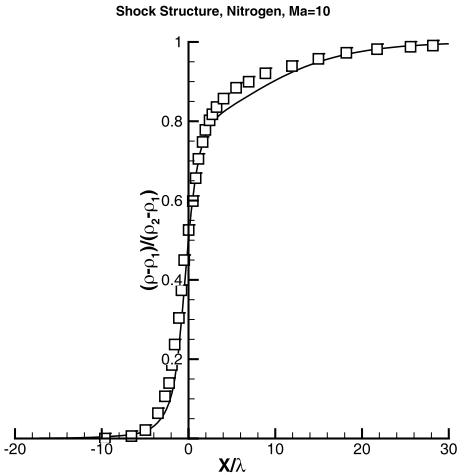

(a) Density

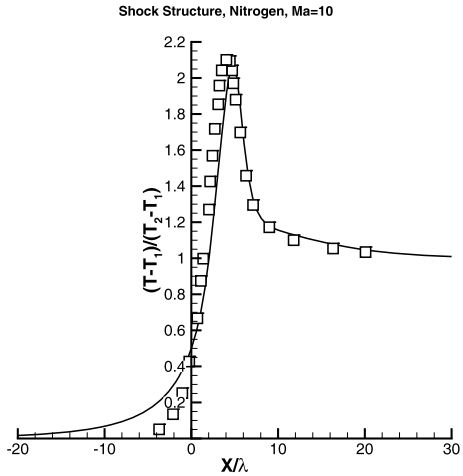

(b) Normal translational temperature

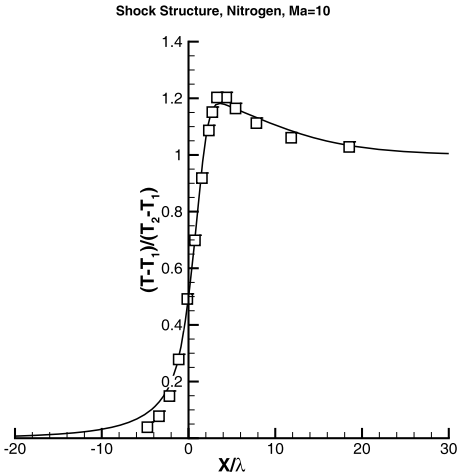

(c) Parallel translational temperature

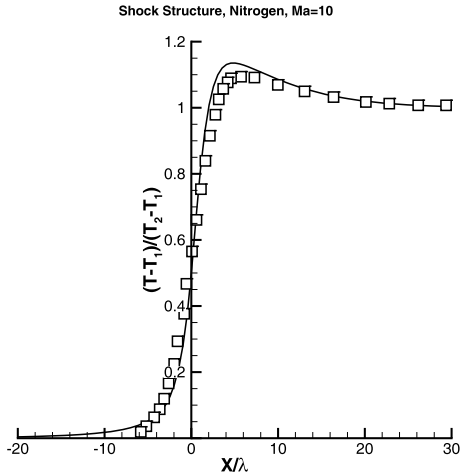

(d) Rotational temperature

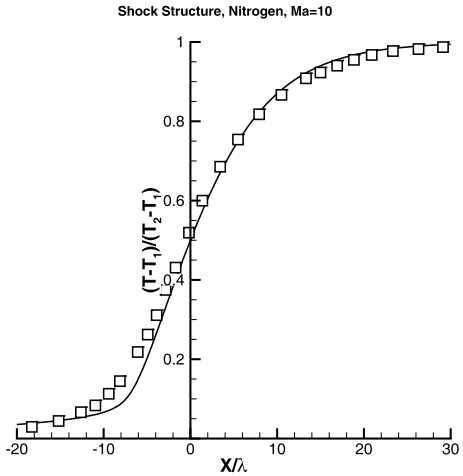

(e) Vibrational temperature

Fig. 5. Solutions for nitrogen gas for $Ma = 10.0$ shock structure with ($Zr^* = 3$, $Zv^* = 40$). All x-coordinates and physical quantities are dimensionless. Square: DSMC, solid line: UGKS-Vib.

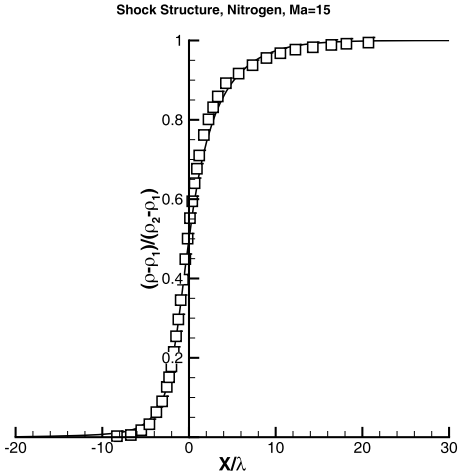

(a) Density

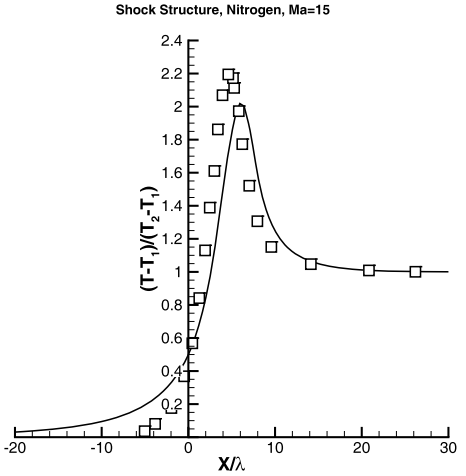

(b) Normal translational temperature

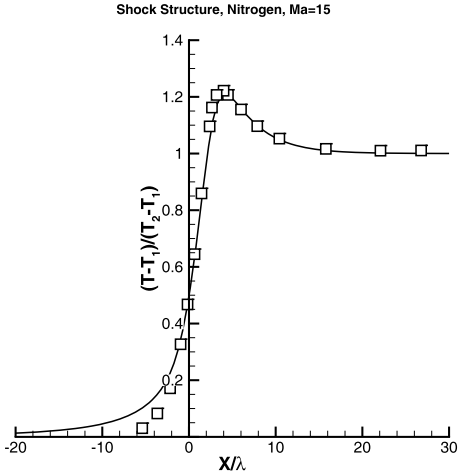

(c) Parallel translational temperature

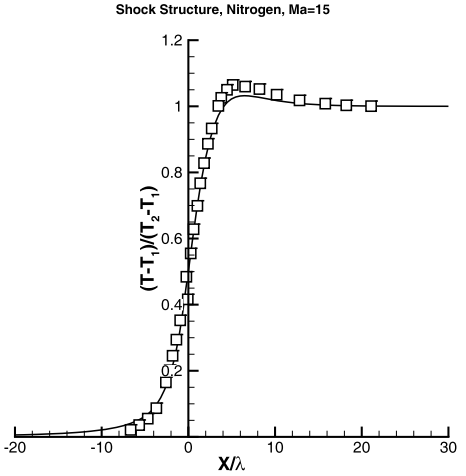

(d) Rotational temperature

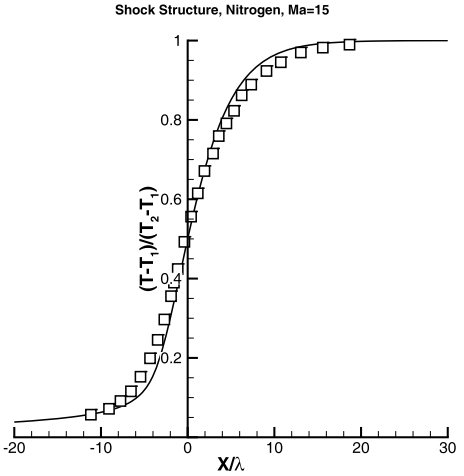

(e) Vibrational temperature

Fig. 6. Solutions for nitrogen gas for $Ma = 15.0$ shock structure with ($Zr^* = 5$, $Zv^* = 20$). All x-coordinates and physical quantities are dimensionless. Square: DSMC, solid line: UGKS-Vib.

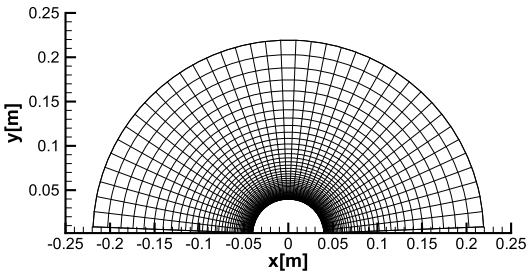

Fig. 7. Computational mesh for nitrogen gas around circular cylinder at $Ma = 15.0$ and $Kn = 0.01$.

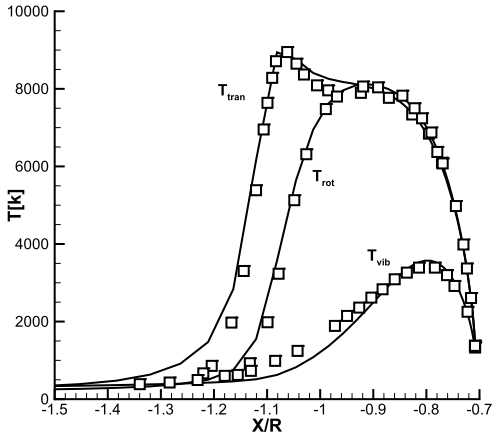

Fig. 8. Flow distributions for nitrogen gas along the 45° extraction line at $Ma = 15.0$ and $Kn = 0.01$. Square: DSMC [38], solid line: UGKS-Vib.

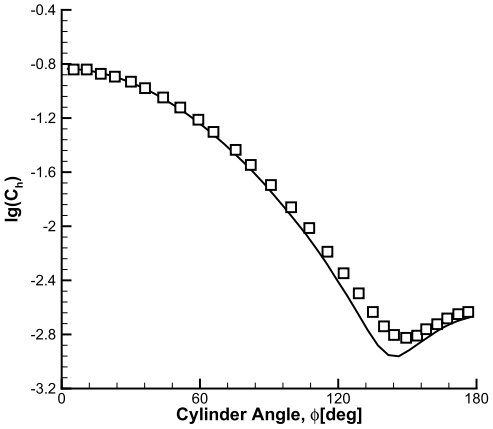

Fig. 9. Surface heating coefficient for nitrogen gas flow around a circular cylinder at $Ma = 15.0$ and $Kn = 0.01$. Square: DSMC [38], solid line: UGKS-Vib. Φ is the angle from the stagnation point.

where K_t, K_r and K_v are the degrees of freedom of nitrogen gas for the translational, rotational, and vibrational ones respectively, with $Zr^{\infty} = 12.5$, $T^* = 91.5$ K, $C_1 = 3$, and $C_2 = 220$.

The comparisons between UGKS-Vib and DSMC solutions are plotted in Figs. 8 and 9. Fig. 8 shows the translational, rotational, and vibrational temperature along the 45° extraction line, in which the rotational and vibrational temperature are matched very well, while the translational temperature profile in UGKS-Vib solution raises up earlier than that in DSMC solution. This is consistent with the previous results of BGK-type models [15]. Fig. 9 shows the surface heating coefficient for nitrogen gas flow around circular cylinder from both UGKS-Vib and DSMC calculations. Reasonable agreement have been achieved.

Table 1
Mesh distributions around a semi-circular cylinder.

Zone	Grid	Y1/mm	Stretch ratio
1	15×55	0.1	1.1
2	60×55	0.1	1.1
3	15×60	0.1	1.1

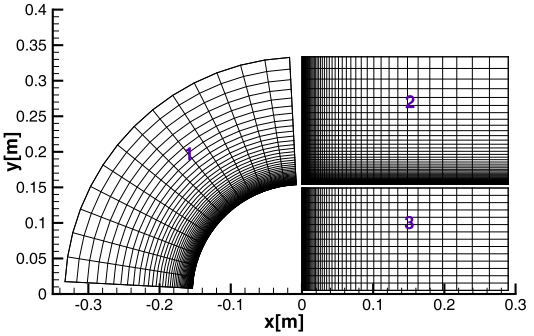

Fig. 10. Computational mesh for nitrogen gas around semi-circular cylinder at $Ma = 10.0$ and $Kn = 0.05$.

3.5. Flow around a semi-circular cylinder

A hypersonic flow passing through a semi-circular cylinder at $Ma = 10.0$ and $Kn = 0.05$ is considered. As shown in Fig. 10, the cylinder radius has a value 0.1542 m, and the computational domain is divided into 3 zones. The detailed mesh information is shown in Table 1, in which Y1 is the height of the first layer of the mesh near the wall, and the stretching ratio is for the mesh in the radial direction.

The inflow nitrogen gas has a velocity $U_\infty = 2883$ m/s with temperature $T_\infty = 200$ K, and molecular mass density $\rho_\infty = 3.949 \times 10^{-6}$ kg/m^3. The semi-circular cylinder has a cold surface with a constant temperature $T_w = 500$ K. For UGKS-Vib, the domain $(u, v) \in [-30 \times \sqrt{RT_\infty}, 30 \times \sqrt{RT_\infty}] \times [-30 \times \sqrt{RT_\infty}, 30 \times \sqrt{RT_\infty}]$ in the velocity space is discretized with 89×89 mesh points based on Newton–Cotes rule. The relaxation time is calculated with $\tau = \mu_\infty (T/T_\infty)^\omega / p_{tran}$, and the temperature exponent of the viscosity coefficient $\omega = 0.74$. Fig. 11 shows flow contours for nitrogen flows around a semi-circular cylinder at $Ma = 10.0$ and $Kn = 0.05$. Fig. 12 shows the comparison of temperature distribution along central symmetric line in front of the stagnation point between the semi-circular (UGKS-Vib) and circular cylinder (DSMC) [37]. Fig. 13 shows the comparison of surface pressure, friction, and heating coefficient between the semi-circular (UGKS-Vib) and circular cylinder (DSMC). It can be concluded that the flow properties in Zone 1 between the semi-circular and circular cylinder are absolutely identical. However, in terms of the flow physics, the former and latter ones are different. The flow physics around a semi-circular cylinder is a multiscale one, where the mean free path can be changed gigantically in the front and rare parts of the cylinder. As shown in Fig. 14, for the flow around semi-circular cylinder, the local Knudsen number can cover a wide range of values with five orders of magnitude difference. Here the local Kundsen number is defined as

$$Kn = \frac{\lambda}{L}, \tag{74}$$

where

$$\lambda = \frac{4\alpha(7-2\omega)(5-2\omega)}{5(\alpha+1)(\alpha+2)} \left(\frac{1}{2RT}\right)^{1/2} \frac{\mu}{\rho},$$

and $L = \rho/|\nabla\rho|$ for the hard sphere (HS) model ($\alpha = 1.0, \omega = 0.5$).

It can be seen that the local Knudsen number near the rear wall is very high, which is above 10, especially in the domain of $D_H = (x, y) \in [0, Y1] \times [0.1, 0.1542]$. This simulation demonstrates that the UGKS can solve the multiple scale problem efficiently.

Furthermore, through the streamline in Zone 3, we can see that the density of flow in the domain D_H is quite low due to the expansion wave. So the gas around the symmetric line near rear wall is pushed from behind to the domain D_H. Therefore, as shown in Fig. 15, the friction coefficient on rear wall surface is negative in the vicinity close to Zone 2, which is positive near the symmetric line in Zone 3. In addition, Fig. 16 shows the temperature distributions along central symmetric line near the rear wall. It is observed that the flow in this region is highly non-equilibrium. The translational, rotational, and vibrational temperature are totally different. Among them, the vibrational temperature is almost constant due to the reason that the vibrational degrees of freedom have not been activated under such a low temperature and large local particle collision time. Moreover, the translational temperature is lower than the rotational temperature due to the

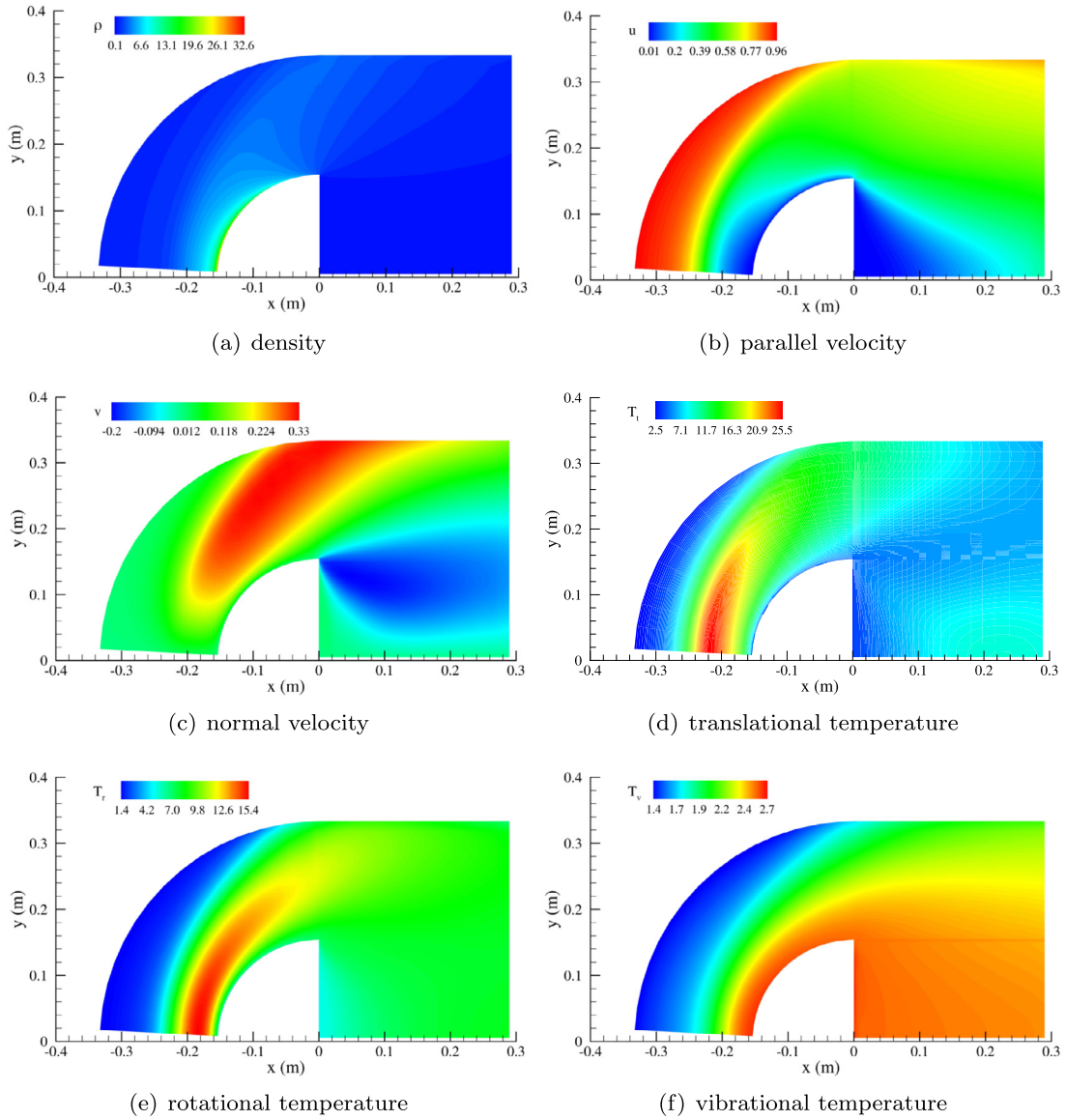

(a) density (b) parallel velocity

(c) normal velocity (d) translational temperature

(e) rotational temperature (f) vibrational temperature

Fig. 11. Flow contours for nitrogen flows around a semi-circular cylinder at $Ma = 10.0$ and $Kn = 0.05$.

translational temperature reduction from the high flow expansion, and its inefficiency to exchange energy with the rotational and vibrational ones. Also, due to the short relaxation time for the translational mode, the translational temperature is closer to the wall temperature than the rotational one.

In summary, the flow around semi-circular cylinder is associated with multiscale flow physics. The particle mean free path can be changed several orders of magnitude from the front to the rear parts. The UGKS is suitable method for flow simulation with the existence of multiple flow regimes.

4. Conclusions

In this paper, a unified gas-kinetic scheme with vibrational relaxation is developed for the non-equilibrium flow simulation of diatomic molecules. The current UGKS is based on a phenomenological model equation with translational, rotational, and vibrational relation and different relaxation times. Through the adoption of the time dependent integral solution of the kinetic model equation for the flux evaluation, the UGKS incorporates the flow physics from the particle free transport in the kinetic scale to the equilibrium formation in the hydrodynamic scale. As a result, the UGKS can simulate flows in all regimes without the requirement on the mesh size being less than the particle mean free path. The new scheme with vibrational mode has been tested in five cases, i.e. relaxation of homogeneous flow, shock structure calculations, shock tube problem, and hypersonic flow passing through a circular and semi-circular cylinders. The numerical results are compared

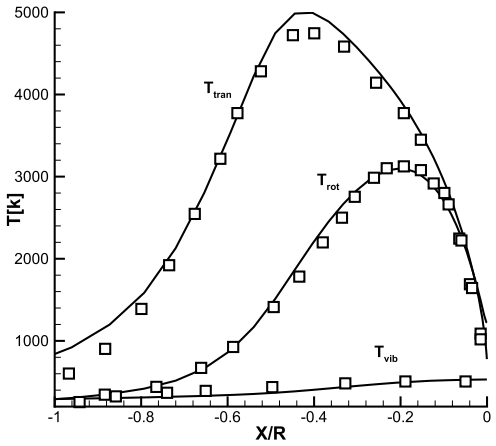

Fig. 12. Flow distributions for nitrogen gas along central symmetric line in front of the stagnation point at $Ma = 10.0$ and $Kn = 0.05$. Square: circular cylinder (DSMC), solid line: semi-circular cylinder (UGKS-Vib).

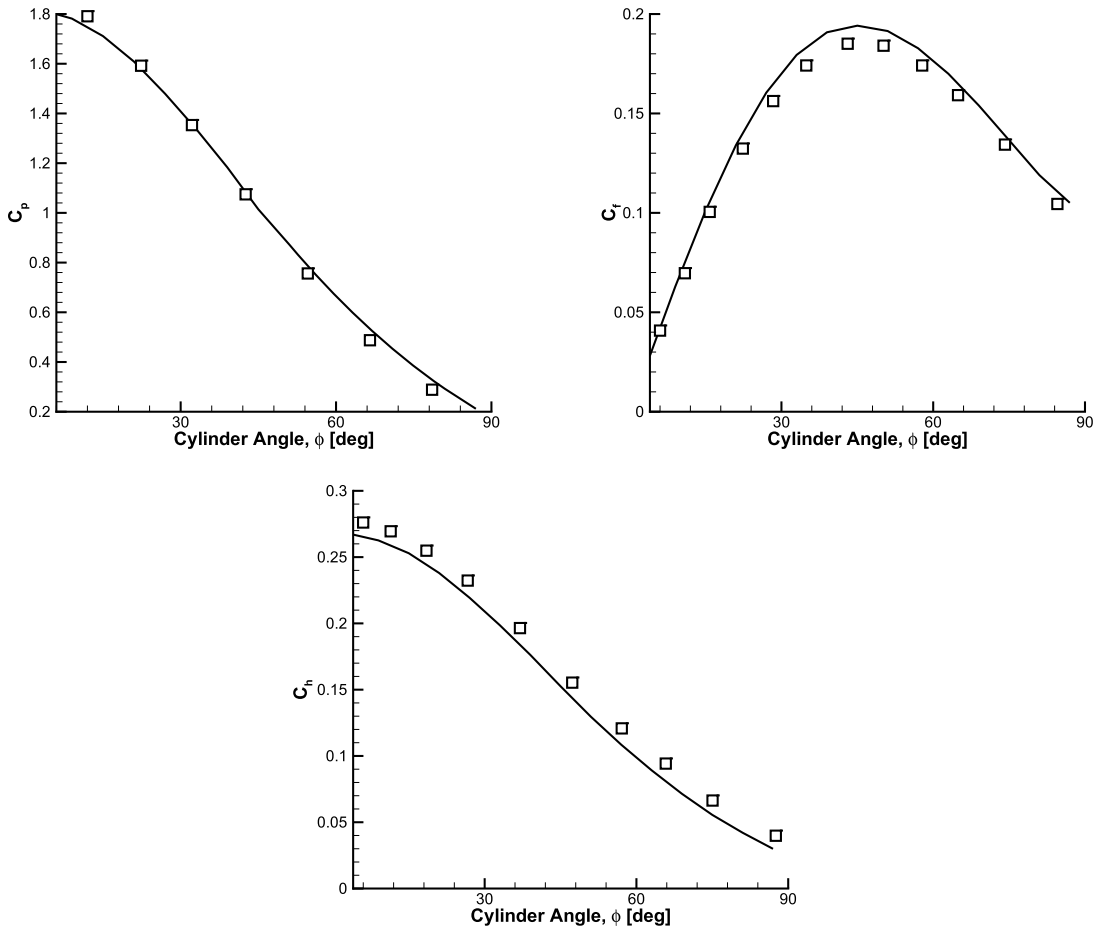

Fig. 13. Surface pressure, friction, and heating coefficient for nitrogen gas flow around circular cylinder at $Ma = 10.0$ and $Kn = 0.05$. Square: circular cylinder (DSMC), solid line: semi-circular cylinder (UGKS-Vib). Φ is the angle from the stagnation point.

with the analytical solutions and DSMC computations. Reasonable agreements between UGKS and other validated solutions have been obtained. In order to further develop the scheme for engineering applications, the vibrational relaxation with quantum energy levels will be implemented into UGKS in the future.

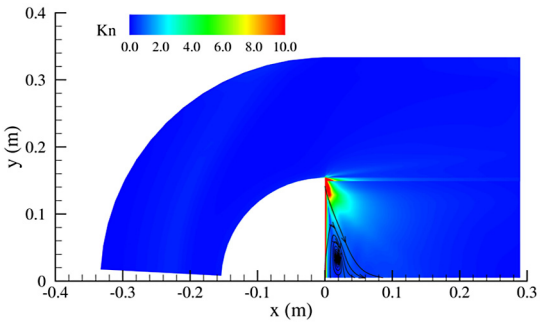

Fig. 14. The local Knudsen number contour for nitrogen gas flow around semi-circular cylinder at $Ma = 10.0$ and $Kn = 0.05$.

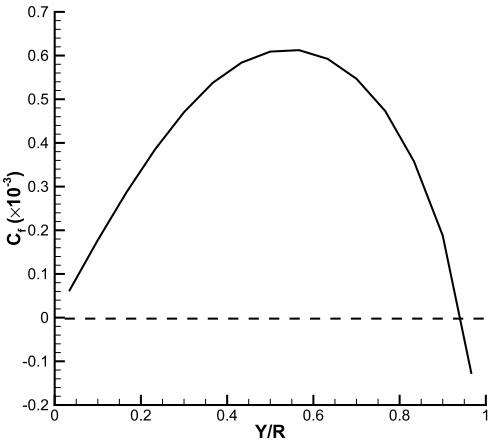

Fig. 15. The rear wall surface friction coefficient for nitrogen gas flow around circular cylinder at $Ma = 10.0$ and $Kn = 0.05$.

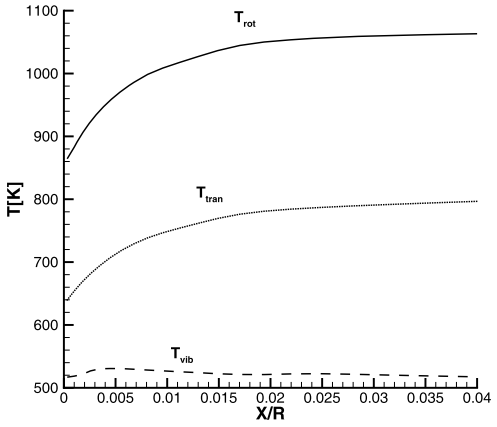

Fig. 16. Temperature distributions for nitrogen gas along central symmetric line near the rear wall at $Ma = 10.0$ and $Kn = 0.05$.

Acknowledgements

The project is supported by National Natural Science Foundation of China under grant No. 11672242 and supported by Science Challenge Project under grant No. TZ2016001. The research of K. Xu is supported by Hong Kong research grant council (16207715, 16211014) and NSFC–91330203 and 91530319.

References

[1] G.A. Bird, Molecular Gas Dynamics and the Direct Simulation of Gas Flows, vol. 242, Clarendon, 1994.
[2] D. Jiang, Study of the Gas-Kinetic Scheme Based on the Analytic Solution of Model Equations, Ph.D. thesis, China Aerodynamics Research and Development Center, 2016.

[3] Z.-H. Li, H.-X. Zhang, Gas-kinetic description of shock wave structures by solving Boltzmann model equation, Int. J. Comput. Fluid Dyn. 22 (9) (2008) 623–638.
[4] Z.-H. Li, H.-X. Zhang, Gas-kinetic numerical studies of three-dimensional complex flows on spacecraft re-entry, J. Comput. Phys. 228 (4) (2009) 1116–1138.
[5] S. Schlamp, B.C. Hathorn, Higher moments of the velocity distribution function in dense-gas shocks, J. Comput. Phys. 223 (1) (2007) 305–315.
[6] A. Aimi, M. Diligenti, M. Groppi, C. Guardasoni, On the numerical solution of a bgk-type model for chemical reactions, Eur. J. Mech. B, Fluids 26 (4) (2007) 455–472.
[7] M.J. Goldsworthy, M.N. Macrossan, M. Abdel-Jawad, Multiple reactions and trace species in the direct simulation Monte Carlo macroscopic chemistry method, Phys. Fluids 19 (11) (2007) 116102.
[8] Z.-H. Li, Z.-H. Li, J.-L. Wu, A.-P. Peng, Coupled Navier–Stokes/direct simulation Monte Carlo simulation of multicomponent mixture plume flows, J. Propuls. Power 30 (3) (2014) 672–689.
[9] C.E. Treanor, J. Rich, R. Rehm, Vibrational relaxation of anharmonic oscillators with exchange-dominated collisions, J. Chem. Phys. 48 (4) (1968) 1798–1807.
[10] K.N.C. Bray, Vibrational relaxation of anharmonic oscillator molecules: relaxation under isothermal conditions, J. Phys. B, At. Mol. Phys. 1 (4) (1968) 705.
[11] M. Capitelli, C.M. Ferreira, B.F. Gordiets, A.I. Osipov, Plasma Kinetics in Atmospheric Gases, vol. 31, Springer Science & Business Media, 2013.
[12] C. Cai, D.D. Liu, K. Xu, One-dimensional multiple-temperature gas-kinetic Bhatnagar–Gross–Krook scheme for shock wave computation, AIAA J. 46 (5) (2008) 1054–1062.
[13] V. Aristov, Direct Methods for Solving the Boltzmann Equation and Study of Nonequilibrium Flows, vol. 60, Springer Science & Business Media, 2001.
[14] K. Xu, J.-C. Huang, A unified gas-kinetic scheme for continuum and rarefied flows, J. Comput. Phys. 229 (20) (2010) 7747–7764.
[15] C. Liu, K. Xu, Q. Sun, Q. Cai, A unified gas-kinetic scheme for continuum and rarefied flows IV: full Boltzmann and model equations, J. Comput. Phys. 314 (2016) 305–340.
[16] J.-C. Huang, K. Xu, P. Yu, A unified gas-kinetic scheme for continuum and rarefied flows II: multi-dimensional cases, Commun. Comput. Phys. 12 (03) (2012) 662–690.
[17] J.-C. Huang, K. Xu, P. Yu, A unified gas-kinetic scheme for continuum and rarefied flows III: microflow simulations, Commun. Comput. Phys. 14 (05) (2013) 1147–1173.
[18] S. Chen, K. Xu, C. Lee, Q. Cai, A unified gas kinetic scheme with moving mesh and velocity space adaptation, J. Comput. Phys. 231 (20) (2012) 6643–6664.
[19] S. Liu, C. Zhong, Modified unified kinetic scheme for all flow regimes, Phys. Rev. E 85 (6) (2012) 066705.
[20] E. Shakhov, Generalization of the Krook kinetic relaxation equation, Fluid Dyn. 3 (5) (1968) 95–96.
[21] S. Liu, P. Yu, K. Xu, C. Zhong, Unified gas-kinetic scheme for diatomic molecular simulations in all flow regimes, J. Comput. Phys. 259 (2014) 96–113.
[22] V. Rykov, A model kinetic equation for a gas with rotational degrees of freedom, Fluid Dyn. 10 (6) (1975) 959–966.
[23] H. Zhang, A Unified Gas-Kinetic Scheme Based on a Vibrational Model, Master's thesis, Northwestern Polytechnical University, 2015.
[24] P.L. Bhatnagar, E.P. Gross, M. Krook, A model for collision processes in gases. I. Small amplitude processes in charged and neutral one-component systems, Phys. Rev. 94 (3) (1954) 511.
[25] M. Kogan, On the equations of motion of a rarefied gas, J. Appl. Math. Mech. 22 (4) (1958) 597–607.
[26] L.H. Holway Jr, New statistical models for kinetic theory: methods of construction, Phys. Fluids 9 (9) (1966) 1658–1673.
[27] Y. Zheng, H. Struchtrup, Ellipsoidal statistical Bhatnagar–Gross–Krook model with velocity-dependent collision frequency, Phys. Fluids 17 (12) (2005) 127103.
[28] K. Xu, Regularization of the Chapman–Enskog expansion and its description of shock structure, Phys. Fluids 14 (4) (2002) L17–L20.
[29] K. Xu, L. Tang, Nonequilibrium Bhatnagar–Gross–Krook model for nitrogen shock structure, Phys. Fluids 16 (10) (2004) 3824–3827.
[30] K. Xu, E. Josyula, Continuum formulation for non-equilibrium shock structure calculation, Commun. Comput. Phys. 1 (3) (2006) 425–448.
[31] K. Xu, A generalized Bhatnagar–Gross–Krook model for nonequilibrium flows, Phys. Fluids 20 (2) (2008) 026101.
[32] K. Xu, X. He, C. Cai, Multiple temperature kinetic model and gas-kinetic method for hypersonic non-equilibrium flow computations, J. Comput. Phys. 227 (14) (2008) 6779–6794.
[33] C. Chu, Kinetic–theoretic description of the formation of a shock wave, Phys. Fluids 8 (1) (1965) 12–22.
[34] K. Xu, A gas-kinetic bgk scheme for the Navier–Stokes equations and its connection with artificial dissipation and Godunov method, J. Comput. Phys. 171 (1) (2001) 289–335.
[35] L. Wu, C. White, T. Scanlon, J. Reese, Y. Zhang, A kinetic model of the Boltzmann equation for non-vibrating polyatomic gases, J. Fluid Mech. 763 (2015) 24–50.
[36] O. Tumuklu, Z. Li, D.A. Levin, Particle ellipsoidal statistical Bhatnagar–Gross–Krook approach for simulation of hypersonic shocks, AIAA J. (2016) 3701–3716.
[37] A.J. Lofthouse, Nonequilibrium Hypersonic Aerothermodynamics Using the Direct Simulation Monte Carlo and Navier–Stokes Models, Tech. rep., Michigan Univ., Ann Arbor, 2008.
[38] T.R. Deschenes, Extension of a Modular Particle-Continuum Method for Nonequilibrium, Hypersonic Flows, Ph.D. thesis, University of Minnesota, 2011.